1967

Buckling and ultimate loads for plate girder webs under edge load, June 1967 M.S. for Bossert

A. Ostapenko

T. W. Bossert

BUCKLING AND ULTIMATE LOADS FOR PLATE GIRDER WEB PLATES UNDER EDGE LOADING

by

Theodore W. Bossert

and

Alexis Ostapenko

Fritz Engineering Laboratory
Department of Civil Engineering
Lehigh University
Bethlehem, Pennsylvania

June 1967

Fritz Engineering Laboratory Report No. 319.1

TABLE OF CONTENTS

ABSTRACT

This investigation is a study of the buckling and ultimate strength of the web plate of a plate girder subjected to vertical compressive load bearing through the compression flange between transverse stiffeners. The effect of the compressive load combined with bending and shear stresses was considered.

A computer analysis was performed to find the buckling strength of the web plate, and the ultimate strength was found from tests on three girders. The ultimate loads were compared with buckling loads and Formulas 15 and 16 of the 1961 AISC Specification.

The ultimate loads were found to be from three to four times the buckling loads, indicating considerable post-buckling strength. A tentative relation between the buckling and ultimate strength was established incorporating the influence of bending stress and aspect ratio. The investigation showed that the factor of safety based on the AISC Specification reduces considerably with increasing bending stress intensity.

An ultimate strength theory should be developed and more tests performed for various b/t ratios and materials.

1. INTRODUCTION

1.1 Scope

In plate girder construction, current practice has been to place a bearing stiffener at the location of a concentrated load to prevent web crippling or web buckling. There are some situations, however, when the exact location of an expected concentrated load is not knownor cannot be determined. Such a situation occurs in plate girders which support crane rails or railroad tracks directly on top of the compression flange. Since concrete slabs, ties, rails, etc. tend to distribute the load over the panel, uniform loading, such as that shown in Fig. 1 is assumed.

The purpose of this investigation is to study the buckling characteristics and ultimate strength of the web plate when it is subjected to the loading condition described above. Figure 2 shows the web plate of a plate girder panel with the edge loads which would correspond approximately to the loading condition in Fig. 1. The edge loads are those that would occur on a panel under uniform moment and under vertical compression through the top flange. Some consideration will also be made of panels subjected to combined moment, shear and vertical compression, as shown in Fig. 3.

In this paper, the results of the ultimate strength tests and the buckling analysis of the web plate under the loading condition shown in Fig. 2 are presented to see what relation, if any, exists between linear buckling theory and the ultimate strength of the panel. In the tests, the loads shown in Fig. 2 were approximated on panels of various aspect ratios. The z value was also varied throughout the test series. Test specimens and methods of testing are also described.

1.2 Historical Background

A limited amount of work has already been done on the buckling characteristics of plate girder webs under the vertical compressive load, but no test data have been published so far. Wilkesmann, Klöppel, Wagemann, and Warkenthin have done some buckling analyses using energy methods.[1][2][3] In Japan, buckling stresses for simply supported plates have been analyzed in connection with ship structures by Yoshiki, Ando, Yamamoto and Kawai.[4]

The American Institute of Steel Construction issued in 1961 a specification which incorporated provisions for plate girders under loads applied between transverse stiffeners.[5] These provisions are based on an approximate buckling analysis developed by Basler.[6] However, in his analysis, no consideration was given to bending or shear on the plate panel. Only compressive load applied through the compression flange was taken into account.

No other specifications have been introduced to limit vertical compressive stress on a plate girder panel acting through the compression flange.

1.3 General Review of the Problem and Summary of the Investigation

The investigation consisted of two major phases, a theoretical analysis of the buckling behavior of rectangular web plates, and a test program of plate girder panels to determine the ultimate capacity.

The theoretical work was mainly concerned with the buckling behavior of the web plate under the loading shown in Fig. 2. It was assumed that shear stresses on the vertical edges of the web plate were uniform over the depth of the web and that the flange took no transverse shear. This assumption allowed the analysis of the web plate to be independent of the relative sizes of the flange and web plates. The computer program developed for the analysis can handle other loading conditions as well, for example, the one shown in Fig. 3.

In the panel shown in Fig. 2, the parameter z is the ratio of the maximum compressive bending stress, σ_b, to the vertical compressive stress, σ_c. During the analysis of a web plate under a particular edge loading distribution, the loads are assumed to be proportional, and the critical load is assumed to be that value of σ_c which, together with proportional bending and shear loads,

causes the plate to buckle. The buckling coefficient was determined for various values of z and the aspect ratio of the plate panel, α. The relationship between the buckling coefficient, k, and the buckling stress is

$$\sigma_{cr} = \frac{\pi^2 E}{12(1-\nu^2)} \left(\frac{t}{b}\right)^2 k \qquad (1.1)$$

where

E = modulus of elasticity

ν = Poisson's ratio

t = plate thickness

b = vertical dimension of the plate

To see what relationship, if any, exists between buckling and ultimate strengths of web plates of plate girders, ten tests on three plate girders were conducted during the fall of 1966 and the winter of 1966-1967. The primary purpose of these tests was to determine the following:

- amount of the post-buckling strength,
- variation of the post-buckling strength with respect to the two variables, z and α,
- the appearance and the behavior of the failed web plate to guide anyone desiring to formulate an ultimate strength theory for web plates under this type of loading.

The secondary purposes were to find out how the failure of the web panel affects the overall behavior of the plate girder, to see what the variation of lateral deflection vs. load was, whether or not the actual buckling loads could be verified from the tests, and to see how edge loading through the compression flange affects other modes of failure typical for plate girders. The testing program is described in more detail in the next chapter.

2. DESCRIPTION OF TESTS

2.1 Description of Test Specimens

Three plate girders were tested; two were 30 feet long, and one--25 feet. In the test section, the girders had 8" by 5/8" flanges and a 36" by 1/8" web as shown in Fig. 6b. Thus, the slenderness ratio, β, in the test section was 288. In all three girders, the end panels had a 3/16" web whose purpose was to prevent any premature failures in the end panels due to high shear. Two girders had three test panels each. In one, the test panel had $\alpha = 0.8$, in the other $\alpha = 1.2$. The third girder had two panels of $\alpha = 1.6$. Table 1 summarizes the basic properties and dimensions of the plate girders. Figures 5a, 5b, and 6a are side views of the plate girders showing basic dimensions, stiffener sizes and placement, and the location of web splices. Figure 6b shows the girder cross sections at locations indicated on Figs. 5a, 5b, and 6a. The types of stiffeners and locations of welds between stiffeners and other plate elements are also indicated in Fig. 6b. Table 2 gives the significant material properties obtained from tensile specimen tests which will be described in the next chapter.

The original intent was to have homogeneous girders with the yield stress of 36 ksi throughout, but the web turned out to have a higher yield stress than desired, despite considerable efforts

to match yield stresses by means of hardness tests on the plate elements during their selection. The difference in yield stresses between the flanges and the web produced an unfavorable condition for panels tested under heavy bending.

The test specimens had relatively large initial web deflections due to the slenderness of the web and a fabrication procedure which was not as successful in preventing initial deformations as was hoped.

2.2 Instrumentation

Instrumentation was needed to measure lateral deflections of the web, vertical deflection of the entire plate girder, and strains at a number of points on the girder surface. Correspondingly, the instrumentation consisted of a dial gage rig and strain gages.

The dial gage rig, shown in Fig. 7, was used for measuring web plate deflections relative to the top and bottom flanges. It was applied at several stations along the test panel and at some stations at neighboring panels. The rig was originally designed to measure lateral deflections on 50 inch girders which were tested several years ago for another project. For the 36 inch girders in these tests, it was modified to the one shown in the figure. Figure 7 shows the dial rig in the proper position for lateral deflection measurement. The dial gages had the finest division of one thousandth of an inch. A set of lateral deflection measurements was taken after each increment of load.

For strain measurement, linear SR4, A-1-SX* gages and SR-4 AR-1* rosettes were used. The gage length of the linear gages was 13/16 inch, for the rosettes--3/4 inch. The estimated accuracy for this type of gage is about 1%. Most of the gages and rosettes were placed so that edge stresses in the panels could be measured. The most significant gages were those at the top edge of the test panel which gave the vertical compressive stress distribution in the web. The placement of strain gages for typical test panels is shown in Fig. 8. Other panels had fewer rosettes along the sides. There were also some rosettes placed in the interior of some of the test panels to detect the occurrence of any unusual stress conditions. The number of gages was limited because of the expense and the limit on the number of channels available on the strain gage indicators.

The strains were digitized by a Budd** strain gage indicator which allowed reading of the strains directly when the unit was switched to a particular strain gage.

The installation of the strain gages on the plate girder, and the wiring of the gages to the indicators was a very time consuming operation. In future tests this job should be started as early as possible to avoid delays in testing.

* Company that made gages was Baldwin-Lima-Hamilton
**Manufactured by Instruments Division of Budd Company

The loads were applied with Amsler* 110 kip and 55 kip jacks which have a five inch stroke for static testing. The loads were measured with Amsler* pendulum dynamometers which provide both the hydraulic pumping mechanism to apply the load and a mechanism for measuring it. The scale on the pendulum dynamometer can be adjusted so that when the indicator is at full scale, the jack is exerting its full capacity. Thus, 55 kip or 110 kip jacks can be used without loss of accuracy in load measurement.

A dial gage under the girder was used to measure the vertical deflection in order to give an indication of the overall behavior of the girder. Also, a dial gage was mounted near the top of the plate girder is shown in Fig. 9 to indicate the lateral movement of the web. This gage was not necessarily an accurate measure of the web deflection at this point, since the flange to which it was fastened could twist. However, it was sufficiently accurate to detect the advent of web failure. Lateral deflections were also measured at the same point with the dial rig. Twisting of the top flange was sometimes caused by eccentricity of the vertical compressive load in relation to the line of the web, and usually it was relatively sudden. To detect the flange twisting, a level was placed on top of the flange and the movement of the bubble observed.

*Manufactured by Alfred J. Amsler Co., Schaffhouse, Switzerland

2.3 Test Set-Ups and Loads

The basic set-ups for all of the tests are shown schematically in Figs. 10, 11 and 12. All loads which were not placed directly over the test panel were used to subject the panel to a greater moment (and shear) than that provided by the load over the test panel alone. In Fig. 13 are photographs of two of the test set-ups used in the test series.

The girders were braced at each transverse stiffener against lateral-torsional buckling of the top flange, as shown in Fig. 13b. Despite this, some lateral buckling did occur in tests where the flange was subjected to high stresses resulting from heavy bending of the plate girder. The bracing consisted of pipes fastened to the stiffeners with a hinged connection as shown in Fig. 14. These pipes were supported at the other end by a beam, which was bolted to columns of the building.

As was mentioned in Section 2.2, loads were applied with Amsler hydraulic jacks acting in conjunction with Amsler pendulum dynamometers. In some tests, two independent loads were applied with two pendulum dynamometers so that the desired proportions between the loads could be obtained. It was possible and practical for one man to operate the two pendulum dynamometers simultaneously during the period when the load was to be maintained at a constant level, but during loading and unloading, a separate man was needed to operate each dynamometer, since loading

of one dynamometer would unload the other because of the deflection of the plate girder.

The load over the test panel was distributed as shown in Figure 13, 14, and 15b. The bearing plates on the top flange were of sufficient size to prevent local web crippling. This did not provide an exactly uniform load distribution, but it did provide a loading situation which was somewhat more severe. The loading mechanism also allowed all of the load to be carried by the web so that none of it went directly into the stiffeners at the side edges of the panel.

In one test, EG-2.2, a wood beam was used in an attempt to distribute the load more evenly as shown in Fig. 15a. However, this was found to be unsatisfactory because the beam transmitted some of the load to the stiffeners. Also, it acted compositely with the plate girder thus reducing the bending stress at the top of the test panel.

It can be seen from the photographs in Fig. 15 that a brace was needed to stabilize the load distributing mechanism. This was necessary on all of the tests on EG-3, and in test EG-2.2. One or two pipes were fastened to the loading beam directly under the jack to provide stability in the load distributing mechanism and to prevent damage to the girder if twisting of the flange should take place.

2.4 Testing Procedure

Basically, the testing procedure for all of the tests was the same. For each test the loads were kept proportional. First, zero readings were taken for all strain and dial gages. To measure the initial deflections of the web a set of lateral deflection readings was taken at the desired locations along the girder and compared to readings on a flat machined surface. The zero readings for each dial were subtracted from the corresponding dial readings taken on the girder, thus giving the lateral deflections at the points where the dial gages were located. Upon one placement of the dial rig at a station on the girder, the lateral deflection was measured at seven points along a vertical line. The measurement was performed at from four to six horizontal locations, or stations, along the test panel and at about three to six stations outside the test panel on adjacent panels.

After all zero strain readings and initial deflection readings were taken, the first load (P = 2 kips) was applied. During the application of the first load, the jacks were lined up so that they acted directly over the center line of the web. This was designed to reduce the possibility of twisting of the flange due to eccentricity of the load. This operation was done by eye; therefore there was always some uncertainty about the accuracy of the alignment. As the test progressed, the load increment was

held constant at two, three, or four kips, depending on the expected ultimate load on the panel, which could be between 30 and 55 kips, depending on the bending stress and the aspect ratio of the panel. Usually, when inelastic behavior was detected in the web or in the plate girder as a whole, the load increment was cut to one kip or one-half kip. The load then was held constant and the reading deferred until the needle on the dial gage measuring lateral deflection stopped moving. A set of strain gage and lateral deflection readings were taken, and the load increased by one-half kip. Usually, the dial needle would move a few divisions during the reading, but at this point, lateral deflections of the web were so large that this change was negligible. Failure was defined by the formation of a band of yielding as shown in the photograph in Fig. 16. The band is indicated by the arrows. After the formation of the yield band, the panel could not carry any higher load.

In some cases under high bending, the test was stopped before the formation of the yield band because of the lateral buckling of the top flange. This was done to prevent too much permanent distortion in the top flange, which would make aligning of the jacks with the web difficult for further tests on the girder. The same panel was later tested to failure with a somewhat lighter bending stress.

In most of the tests, the girder was unloaded gradually, with sets of readings taken at ten to fifteen kip increments in order to establish the unloading curve.

3. THEORY

3.1 Introduction

In this section, an explanation of the buckling analysis and equations used in the computer program are presented. The first part of the chapter is devoted to the finite difference method of determining stresses in the plate due to edge loading. In the second part of the chapter, the finite difference method for determining the buckling coefficient from the resulting plane stress distribution is given. In both the stress and buckling analyses, the basic equations, the finite difference operators and their use, the methods used for dealing with the boundary conditions, and any necessary matrix operations are described.

3.2 Finite Difference Operators for the Plane Stress Analysis

For the purpose of analysis, the web plate panel is subdivided into a mesh as shown in Fig. 4.

It can be shown that

$$\nabla^4 \phi = 0 \tag{3.1}$$

or

$$\frac{\partial^4 \phi}{\partial x^4} + 2 \frac{\partial^4 \phi}{\partial x^2 \partial y^2} + \frac{\partial^4 \phi}{\partial y^4} = 0 \tag{3.1a}$$

satisfies the equilibrium and compatibility equations associated

with the plane stress problem of the theory of elasticity.[7] ϕ is the Airy Stress Function, as given by the following definitions.

$$\sigma_x = \frac{\partial^2 \phi}{\partial y^2} \tag{3.2a}$$

$$\sigma_y = \frac{\partial^2 \phi}{\partial x^2} \tag{3.2b}$$

$$\tau_{xy} = -\frac{\partial^2 \phi}{\partial x \partial y} \tag{3.2c}$$

The finite difference solution of Eq. 3.1 gives values of ϕ at discrete points on the plate, called "nodal points" or "mesh points". Mesh points for this problem are designated by the numbering system shown in Fig. 4. One can approximate Eq. 3.1a at a mesh point designated by the numbers m, and n by the following expression:

$$\frac{1}{d_2^4}\Big[\gamma^4(\phi_{m+2\ n} + \phi_{m-2\ n}) + \phi_{m\ n+2} + \phi_{m\ n-2} + (6\gamma^4 + 8\gamma^2 + 6)\phi_{m\ n} + 2\gamma^2(\phi_{m-1\ n-1} + \phi_{m-1\ n+1} + \phi_{m+1\ n-1} + \phi_{m+1\ n+1}) - 4\gamma^2(1+\gamma^2)(\phi_{m-1\ n} + \phi_{m+1\ n}) - 4(1+\gamma^2)(\phi_{m\ n+1} + \phi_{m\ n-1})\Big] = 0 \tag{3.3}$$

where γ is d_2/d_1

d_1 is distance between mesh points in y direction

d_2 is distance between mesh points in x direction

If Eq. 3.1 is written in the finite difference form for every interior mesh point on the plate, a set of linear simultaneous equations is developed which can be solved for the $\emptyset$ value at each mesh point on the plate. An easy way of writing this equation is to draw a representation of this operator, called a "star" or "molecule" and apply it to each point. Such a star is shown in Fig. 17. This is done by mentally placing the center "box" of the star over the mesh point that is to be operated on, and assigning the values in the "boxes" as coefficients to unknown $\emptyset$ values covered by the boxes. All coefficients of $\emptyset$ values not covered by a box are assigned the value of zero.

If this procedure is applied to all of the points inside the plate, the desired set of linear simultaneous equations will be obtained. When the star is applied to mesh points near the plate edge, some of the boxes fall on the plate edge and on imaginary mesh points outside the plate. Since these stress function values depend on edge loads, the set of simultaneous equations is not homogeneous, and thus it can be solved directly. The determination of the stress function values on the edge will be discussed next.

3.3 Stress Function Values for Mesh Points on the Plate Edge

Although the determination of the values at the edge is a straight forward mathematical procedure, it is somewhat tricky. Since to the author's knowledge, it has not been described anywhere in detail, the procedure will be given in this section. The values of the stress function at the edges must be determined by integration of the edge stresses due to loading. The basic equations for performing this integration are found directly from Eqs. 3.2 and basic equilibrium equations.

$$\partial\phi/\partial x = -\int \bar{Y}\, ds + A \tag{3.4a}$$

$$\partial\phi/\partial y = \int \bar{X}\, ds + B \tag{3.4b}$$

$$\phi = x\ \partial\phi/\partial x + \int x\, \bar{Y}\, ds + y\ \partial\phi/\partial y - \int y\, \bar{X}\, ds + C \tag{3.4c}$$

$\bar{X}$ and $\bar{Y}$ are shown on the differential element in Fig. 18a. The discussion will be confined to the application of these equations to a rectangular plate with the coordinate axes shown in Fig. 4. However, the analysis presented here is valid for any placement of the coordinate axes as long as they are parallel to those shown.

The difficult aspect of this analysis is the sign conventions that must be used for $\bar{X}$ and $\bar{Y}$. Consider first the lower and right edges of the plate. Since ds is positive counterclockwise, as shown in the element in Fig. 18a, ds = dx on the bottom edge,

and ds = dy on the right edge of the plate.

The general expressions for $\bar{X}$ and $\bar{Y}$ are

$$\bar{X} = \sigma_x \cos(N,x) + \tau_{xy} \cos(N,y) \tag{3.5a}$$

$$\bar{Y} = \sigma_y \cos(N,y) + \tau_{xy} \cos(N,x) \tag{3.5b}$$

N is the outer normal to the plate edge

Therefore, along a bottom edge, cos (N,y) = -1, and cos (N,x) = 0; therefore, $\bar{Y} = -\sigma_y$, and $\bar{X} = -\tau_{xy}$. On the right edge, $\bar{Y} = \tau_{xy}$ and $\bar{X} = \sigma_x$. Thus, Eq. 3.4a and 3.4b become:

Bottom edge

$$\partial\phi/\partial x = -\int(-\sigma_y)\,dx + A; \quad \frac{\partial\phi}{\partial y} = -\int \tau_{xy}\,dx + B \tag{3.6a,b}$$

Right edge

$$\partial\phi/\partial x = -\int \tau_{xy}\,dy + A; \quad \frac{\partial\phi}{\partial y} = \int \sigma_x\,dy + B \tag{3.6c,d}$$

This is the form in which these equations were used in the computer program. The sign convention for the stresses is shown on the element in Fig. 18b.

Along the bottom edge, the equation for ϕ (Eq. 3.4c) becomes

$$\phi = x\frac{\partial\phi}{\partial x} + \int x\,\bar{Y}\,dx + y\int \bar{X}\,dx + By - \int y\,\bar{X}\,dx + C \tag{3.7}$$

Along the lower edge, y = 0; therefore, the equation reduces to

$$\phi = x \frac{\partial \phi}{\partial x} - \int x \, \sigma_y \, dx + C \tag{3.8}$$

At the right edge, dy = ds; therefore

$$\phi = - x \int \bar{Y} \, dy + A x + \int x \, \bar{Y} \, dy + y \frac{\partial \phi}{\partial y} - \int y \, \bar{X} \, dy + C \tag{3.9}$$

Since x is constant along this edge,

$$\phi = - x \cancel{\int \bar{Y} \, dy} + Ax + x \cancel{\int \bar{Y} \, dy} + y \frac{\partial \phi}{\partial y} - \int y \, \bar{X} \, dy + C \tag{3.10}$$

$$Ax + C = D \qquad \bar{X} = \sigma_x$$

Thus,

$$\phi = y \frac{\partial \phi}{\partial y} - \int y \, \sigma_x \, dy + D \tag{3.11}$$

In determining $\partial\phi/\partial x$, $\partial\phi/\partial y$, and ϕ at the mesh points on the plate edge, it is desirable to locate the origin of the coordinate axes at a convenient starting point. The starting point can be anywhere; thus for an unsymmetrically loaded plate, the lower left corner was chosen. However, for a symmetrically loaded plate, the center line of the lower plate edge was more suitable. This way, only one-half of a symmetrically loaded plate needs to be analyzed. The points mentioned above were selected for ease of programming for a computer.

A segment of loading is defined as a length of the plate edge over which σ and τ can be given as a continuous function of distance along the edge. If both σ and τ for a whole edge can be expressed as one function, the length of this segment of loading is the length of the edge. For example, in Fig. 2, the whole top edge could be considered a single segment of loading since all edge loads can be expressed as a single analytical function of a distance x along the top edge. If, however, the normal stress in the middle half of the top edge were twice that on the remainder of the edge, the top edge would need to be divided into three segments of loading, one over the right quarter of the top edge, one over the middle section and one over the left quarter, as shown in Fig. 19. If there is a length of plate without load, this length is still considered a segment of loading, but σ and τ are set equal to zero.

At the starting point, A, B, and C are set equal to zero, although they can have any arbitrary values. A function is written for σ and τ on the first segment of loading assuming that the origin of coordinates is at the starting point of the segment of loading. The integrations indicated by Eq. 3.6a and 3.6b are performed. The values of $\partial\phi/\partial x$ and $\partial\phi/\partial y$ at all mesh points within the segment of loading can be obtained by substituting the distance between the mesh point in question and the starting point of the segment of loading. The ϕ values for the mesh points are then determined according to Eq. 3.8. At the end of the segment

of loading, the values of ϕ, $\partial\phi/\partial x$ and $\partial\phi/\partial y$ are found and used as integration constants A, B, and C in the next segment of loading. For the next segment of loading, the functions to be integrated are written using the beginning of this new segment of loading as the new origin of coordinates. The values of ϕ, $\partial\phi/\partial x$ and $\partial\phi/\partial y$ are determined in the same way as before, remembering that the constants A, B, and C must be added according to Eqs. 3.6a, 3.6b and 3.8. When the first corner (the lower right corner) is reached, the analyst proceeds as if he had reached the end of a segment of loading except that Eq. 3.6c, 3.6d and 3.11 instead of Eq. 3.6a, 3.6b and 3.8 are used to determine the ϕ, $\partial\phi/\partial x$, and $\partial\phi/\partial y$ values. At the corner the constants D, A, and B are set equal to ϕ, $\partial\phi/\partial x$ and $\partial\phi/\partial y$, respectively.

Upon reaching the upper right corner, a transformation of the original coordinate axes is made in order to allow a re-use of the procedure just described for the two other edges. One can visualize a three dimensional plot of ϕ with respect to x and y. This can be thought of as a surface over the plate with a slope $\partial\phi/\partial x$ in the x direction and slope $\partial\phi/\partial y$ in the y direction. If the axes were rotated 180 degrees, ϕ would remain unaffected with respect to the rotated axes, and the values of $\partial\phi/\partial x$ and $\partial\phi/\partial y$ would be changed only in sign. Thus, the process of finding the values of ϕ, $\partial\phi/\partial x$ and $\partial\phi/\partial y$ at the mesh points on the top plate edge can be continued by rotating the plate with

respect to the axes 180 degrees so that the top right corner becomes the lower left corner. Thus, the top edge becomes the lower edge, and the left edge becomes the right edge, and the analysis can be continued as if it were started on a new plate. The constants A, B, and C are set equal to $-\partial \phi/\partial x$, $-\partial \phi/\partial y$ and $+\phi$ found in the previous step at the former top corner of the plate. The procedure is continued until all remaining stress function values and derivatives are determined. Since the derivatives at the mesh points on the top and left edges of the plate are desired in terms of the original coordinate axes, the signs of $\partial \phi/\partial x$ and $\partial \phi/\partial y$ found using the rotated axes must be changed. The signs of ϕ itself remain the same.

3.4 Relation of Boundary Stress Function Values and Finite Difference Operator $\nabla^4 \phi = 0$

It was mentioned before that the finite difference operator would have "boxes" which would fall on boundary points and on fictitious mesh points outside the plate. For points on the boundary, the ϕ values are merely multiplied by the coefficient inside the box and added to form the nonhomogeneous constant term in the equation. For points outside the plate the values of ϕ must be found.

It is assumed that the ϕ surface is continuous over the plate edge. Then the relationship between the ϕ value at a point outside the plate and the ϕ value at the nearest interior mesh point can be established from finite differences as:

$$\text{top edge } \phi_o = \phi_L + 2d_1 \left.\frac{\partial \phi}{\partial y}\right|_b$$

$$\text{lower edge } \phi_o = \phi_L - 2d_1 \left.\frac{\partial \phi}{\partial y}\right|_b \qquad (3.12)$$

$$\text{right edge } \phi_o = \phi_L + 2d_2 \left.\frac{\partial \phi}{\partial x}\right|_b$$

$$\text{left edge } \phi_o = \phi_L - 2d_2 \left.\frac{\partial \phi}{\partial x}\right|_b$$

where

ϕ_o is the stress function value at the exterior mesh point

ϕ_L is the stress function value at the interior mesh point located opposite the exterior point

$\frac{\partial \phi}{\partial x}, \frac{\partial \phi}{\partial y}$ = stress function derivatives at the boundary with respect to the original coordinate axes

d_1 = vertical mesh point spacing between the ϕ_o and ϕ_L points

d_2 = horizontal mesh point spacing

From these relationships, the ϕ value of the mesh points outside the plate can be incorporated into the finite difference equations.

3.5 Determination of Stresses

With the solution of the simultaneous equations generated by the finite difference operator $\nabla^4 \phi = 0$, the stress function values of all of the mesh points on the plate are determined. Application of finite difference versions of the relations

between the stress function and the stresses,

$$\sigma_x \approx \frac{\partial^2 \phi}{\partial y^2} = \frac{1}{d_1^2}\left[\phi_{m+1\ n} - 2\phi_{m\ n} + \phi_{m-1\ n}\right]$$

$$\sigma_y \approx \frac{\partial^2 \phi}{\partial x^2} = \frac{1}{d_2^2}\left[\phi_{m\ n+1} - 2\phi_{m\ n} + \phi_{m\ n-1}\right] \qquad (3.13)$$

$$\tau_{xy} \approx -\frac{\partial^2 \phi}{\partial x \partial y} = -\frac{1}{4d_1 d_2}\left[\phi_{m+1\ n+1} + \phi_{m-1\ n-1} - \phi_{m-1\ n+1} - \phi_{m+1\ n-1}\right]$$

for all interior points of the plate yields the stresses at each point.

3.6 Buckling Analysis and Finite Difference Operators

The basic equation for the buckling analysis of a plate obtained from linear buckling theory is[8]

$$\nabla^4 w = \left[\sigma_x \frac{\partial^2 w}{\partial x^2} + 2\,\tau_{xy}\frac{\partial^2 w}{\partial x \partial y} + \sigma_y \frac{\partial^2 w}{\partial y^2}\right] \frac{12(1-\nu^2)}{Et^2} \qquad (3.14)$$

where w is lateral plate deflection.

Two finite difference operators are used for this equation, one to represent $\nabla^4 w$ (Fig. 17) and one to represent the right side of the equation, (Fig. 22).* The same mesh that was used in the stress analysis (Fig. 4) is used here. The procedure used here is basically the same as that used in the stress analysis, except that two sets of coefficients are generated for each point, one set for the left side of the equation and one set for the right

*The star in Fig. 17 is multiplied by $1/d_2^4$ to get $\nabla^4 w$.
The star in Fig. 22 is multiplied by $12(1 - \nu^2)/(Et^2)$.

side. In this manner, a set of homogeneous simultaneous equations is generated. These equations are functions of the lateral deflection w and the stresses.

In Section 1.3 the stipulation was made that all edge stresses were a linear function of the edge compressive load, σ_c. Since the "boxes" of the operator representing the right side of the buckling equation are linear functions of the stresses, they are also linear functions of σ_c. Therefore, the set of equations will have the matrix form:

$$\left[U\right]\left\{w\right\} = \sigma_c \left[V\right]\left\{w\right\} \tag{3.15}$$

U is the matrix of coefficients generated by the operator $\nabla^4 w$

V is the matrix generated by the operator of the right side of the equation

w is the deflection vector

Equation 3.15 is re-arranged into the following form which is then solved by iteration:

$$\left[\left[U^{-1}\right]\left[V\right] - \frac{1}{\sigma_{cr}}\left[I\right]\right]\left\{w\right\} = 0$$

The largest eigenvalue of the matrix $\left[U^{-1}\right]\left[V\right]$ gives the lowest non-zero value of the σ_c stress. This value of σ_c is the desired buckling stress.

3.7 Boundary Conditions

As in the stress analysis, some of the boxes of the operators fall on points on the outside of the plate edge. The boundary conditions considered in the situation at hand were either a fixed edge or a simply supported edge. For simply supported edges, fictitious points outside the edge have a deflection equal in magnitude and opposite in sign to the adjacent mesh points inside the plate. For fixed edges, the deflections at both the inside and outside points are equal in magnitude and sign. These two conditions were incorporated into the finite difference operations.

For the present analysis, the boundary conditions assumed were the following:

Case 1. All edges simply supported

Case 2. Top edge fixed, all others simply supported.

4. TEST RESULTS

4.1 Material Properties

Three coupons from each flange plate and five coupons from each web were tested to determine the yield stresses and other material properties. Figure 20 shows the shape and dimensions of the flange coupons. Figures 21a and 21b show coupons from the web cut in the vertical and horizontal directions, respectively. All coupons had a four inch gage length.

The results of the coupon tests are shown in Table 2. The coupons taken from the flanges behaved in a fashion typical for mild structural steel, as shown in Fig. 23a. A definite horizontal plateau followed by strain hardening should be noted. However, web coupons behaved as shown in Fig. 23b, displaying no flat yield plateau. The static yield load was taken to be the intersection of two straight lines, one parallel to the elastic portion of the load-strain curve starting at 0.002in/in on the strain axis, and the line determined by the lower kink points, which are found by stopping the deformation during a coupon test and letting the load settle down to a static value (see Fig. 23b). The lower values of the percent elongation for web coupons should be also noted. Each value represents an average from at least two coupon tests.

The results show that the web yield stresses were higher than the flange yield stresses. This was an undesirable condition since it limited the value of z that could be used in tests.

4.2 Lateral Web Deflections

The lateral web deflection pattern is of interest for studies on the ultimate and fatigue strength of plate girders. Two important considerations are discussed here, the variation of the lateral deflection at a point with the load, and the shape of the deflected plate.

For panels under light bending, $z \approx 1$, the deflection curves have very little curvature until the ultimate load is approached (see Fig. 24a and 24b). There appears to be no drastic increase in the slope of the curve at the theoretical buckling load. The slope decreases gradually to a horizontal line near the ultimate load. For the case shown in Fig. 25 for heavy bending, $z \approx 4$, there appear to be two quasi-linear sections with the increase in slope occurring at about the point where the flange started yielding under the combination of applied and residual stresses. The yielding was manifested by the flaking off of the whitewash.

In the tests on EG-1 (Fig. 25) the differences can be seen in the slopes of the load-deflection curves for various z values. The lateral deflection for the same edge load is much larger for higher z values, thus causing the formation of the yield band

at a lower load. Thus, an increase in bending stresses leads to a reduction of the ultimate edge load.

The magnitude of the lateral deflection should be also considered. At about half the ultimate load, the web deflected from its initial position from about 1 times its thickness at $\alpha = 0.8$ to about twice its thickness at $\alpha = 1.6$. At working loads, the plate could deflect from 0.5t to 1.0t. In all cases, the point of maximum deflection was in the upper quarter of the plate. A significant consideration here is whether these deflections are large enough to cause unfavorable stress distributions at the flange-to-web connection that would cause failure under repeated loading. Future research may be needed to answer this question.

The second aspect associated with lateral deflections is how the overall panel shape changed with the increasing load. The initial and final lateral deflection patterns can be seen in Fig. 26, 27, and 28 for typical test panels for the three aspect ratios. Figs. 29, 30 and 31 show the lateral deflections over the panel depth taken at the centers of the three test panels for two intermediate loads as well as the zero and ultimate loads. It should be noted that the point of maximum deflection moves up as α decreases. The final basic shape is very much the same for all panels despite large differences in initial deflection. In all cases, primary movement appears to be an extreme outward displace-

ment of the top half of the panel. This movement is most pronounced in the center portion of the panel, while the deflection near the stiffeners remains small. In most cases, the lower half of the web plate showed little lateral movement. Sometimes the final deflection was less than the initial deflection because the lower half of the plate was in tension. Sometimes, this effect was offset by a wrinkling effect caused by the large lateral movement of the top half. One can predict little about the lower half of the web plate unless an accurate analysis taking into consideration initial imperfections is performed. However, these deflections were small compared to the deflections in the top half of the plate, where failure took place.

In tests where the panel was subjected to shear, there was some tension field action in the region of high shear, but the tension field was dissipated in the lower shear region. At the end, the deflected shape had the large outward movement in the top half of the panel, but the movement was not symmetrical as it was in the tests where the compressive vertical load was supplemented by bending alone. The deflections near the high shear end were larger because of the effects of the tension field. However, it is interesting to note that the yield band in the deformed web pattern had the same shape as in the panels subjected to bending.

4.3 Stresses in the Web Plate

An important consideration in the test series was the actual stress distribution in the web plate and a comparison with the distribution assumed in the theoretical analysis. Throughout the test series, some significant differences between the test results and theory were noted due to considerable initial imperfections and a discrepancy between the assumed and actual boundary conditions. These differences will be cited and explained. An evaluation of the vertical compressive load distribution will also be made.

The stresses were obtained from the strain readings of the linear gages and rosettes mentioned in Section 2.2. Membrane stresses are plotted as stresses obtained from the average of the strains from the gages mounted on opposite sides of the web plate. Figures 32 and 33 show two test panels with theoretical edge stress distributions given in dashed lines and actual stress distributions shown by points connected with straight solid lines. On the left edge of both test panels and in the middle of the panel from test EG-2.1, the actual stress near the center of the top half of the panel is lower than the assumed stress. This effect is much more pronounced in the center of the panel from test EG-2.1 (Fig. 33). This is due to a transfer of the stress from the web to the top flange as the top portion of the web moves out. Near the top of the web plate, the bending stress is noticeably larger than the predicted value.

The shearing stresses near the top of the plate are much larger than those predicted by assuming a uniform distribution along the side edge and dividing the shear force by the web area. Most of the shear load in both Fig. 32 and 33 was carried near the top of the web plate. Very little was carried at the bottom. The assumption on which the uniform shear stress distribution is based is that the vertical compressive stress at the stiffener varies in a linear fashion with the vertical distance from its maximum value at the top of the panel to zero at the bottom. Actually, the compressive stress is dissipated considerably faster than this. Even some small tensile stresses in the vertical direction (of the order of 1 ksi) were observed at the bottom of the panel.

As was mentioned in Article 2.3, the vertical compressive load was distributed to the panel through bearing plates in all of the tests except EG-2.2. On panels with α = 0.8 and 1.2, two plates were used, each set at about the third point of the panel. On panels with α = 1.6, four bearing plates were used because the panel was wider, thus making more plates necessary. Figure 34 shows the compressive stress distribution over the top of the test panel for all tests. The agreement with the assumed distribution was not very good. The discrepancy seems to lie mainly in the accuracy of the stress evaluation rather than in the actual condition. The section of the web plate was subjected to severe bending because of the lateral deflection near the top, so that

the average strain of the two gages placed on opposite sides of the web was the average of a large positive number and a large negative one. This could cause the readings to be erratic. Also, localized stresses due to the bearing plates contributed to the errors. However, in most cases, with the exception of test EG-2.2, the total area under the dotted line showing the assumed stress distribution and the area under the plot of the test points is essentially the same indicating that the overall effect on the plate was adequately consistent.

In test EG-3.2, an extremely high vertical stress occurred at one end of the panel. A concentrated load was placed over the stiffener bounding the side of the panel thus causing a very high compressive stress in that region. The purpose of the load was to subject the panel to high shear.

In test EG-2.2, a wood beam was used to distribute the vertical stress more evenly over the top of the test panel. As mentioned in Article 2.3, the wood beam carried too much load to the stiffeners bounding the test panel, thus causing a low vertical stress near the middle of the panel away from the stiffeners. Also, some composite action took place between the girder and the wood beam thus reducing the bending stress in the test panel.

4.4 Vertical Plate Girder Deflections

The vertical delfection of the plate girder at the center line of the test panel was a measure of the general behavior of the girder. In low bending tests, the load vs. deflection curve remained linear up until failure as shown in Fig. 35a and 36a, thus indicating that failure of the test panel had little effect on the general plate girder behavior. On tests of high z where some flange yielding occurred, some flattening of the load vs. deflection curve did take place as shown in Fig. 35b. Figure 36b shows the plot for the shear test EG-3.3. A little flattening did take place at the end thus indicating a little yielding of the flange and possibly some inelastic deflection due to the shear on the panel.

4.5 Ultimate Load

The most important information gained from the test series is the variation of the ultimate load with respect to α and z. The ultimate loads obtained in each test, as well as the ratios of the ultimate load to the buckling load are shown in Table 3.* For a particular aspect ratio, the maximum load does become smaller as z increases. Also, the ratio of the ultimate load to the buckling load remains approximately constant for various z values and a constant α, but the ratio becomes lower as α increases. A comparison of the ultimate load with the buckling load and the AISC specification is discussed in more detail in the next chapter.

*Shown in terms of stress coefficients as explained in Chapter 5.

4.6 Failure Mechanism

The final failure of the test panel was indicated by formation of two bands of yielding across the test panel. The first band, shown in Fig. 16 was almost circular in shape, and formed at the points of maximum deflection on the concave side of the plate. The second band of yielding formed directly under the compression flange, on the other side of the plate. Figures 37a, 37b, and 38 show the locations of the first band on the test panels of all three aspect ratios. The bands are almost circular for α = 0.8 and 1.2, but for α = 1.6, the middle portion has less curvature than the portions near the ends of the panel.

The location of the first yield band did not vary either with z, or with shear stress or with the vertical load distribution. The location of the yield band was at about the same place for all test panels of a given aspect ratio.

For high aspect ratios, the first yield band formed at the same time along the entire length of the test panel. For lower α values, the formation was more gradual, with yielding taking place at the ends of the panel first. In shear tests, propagation of the yield band was much slower, starting at the end of high shear, and moving about half way across the panel; the second half formed more quickly.

The second yield band was due to the extreme bending of the web plate just below the compression flange and was in all cases within an inch of the flange.

This deflection pattern could be a very significant help in an ultimate strength analysis of the web plate because of the predictability of the location of the first band of yielding and because of its dependence only on the aspect ratio and not on the loading condition. Tentatively, such an analysis can be formulated by using a large deflection version of the yield line theory.

4.7 Boundary Conditions

In the test series, the top edge of the web plate was assumed fixed and the other three edges were assumed simply supported. (Case 2 from Article 3.7). It was difficult to evaluate from web behavior how valid these boundary conditions were, but web deflection pattern did give indication that the top edge behaved very nearly as a fixed edge. Therefore, the buckling loads for Case 2 will be used in calculating the ratios of ultimate load to buckling load.

5. COMPARISON OF TEST RESULTS WITH THEORY AND AISC SPECIFICATION

5.1 Introduction

The purpose of this chapter is to compare the results of the tests, the theory, and the AISC Specification, to evaluate the results, and to explain the differences.

5.2 Definitions of K values

All of the results can be expressed in terms of the non-dimensional stress parameter K. The relationship defining this parameter is the following

$$\sigma_c = \frac{P}{A_w} = \frac{\pi^2 E}{12(1-\nu^2)} \left(\frac{t}{b}\right)^2 K \qquad (5.1)$$

where

E = modulus of elasticity

ν = Poisson's ratio

t = plate thickness

b = panel depth

K = the stress parameter

P = load

A_w = area of compression edge of web

Since $\frac{\pi^2 E}{12(1-\nu^2)} \left(\frac{t}{b}\right)^2$ for a plate girder panel is a constant dependent only on the material properties and the slenderness ratio, K is

proportional to σ_c and any value of σ_c can be expressed in terms of K. Thus, the following quantities are defined:

$$K = 12\sigma_c \Big/ \left[\frac{\pi^2 E}{(1-\nu^2)}\left(\frac{t}{b}\right)^2\right] \tag{5.2a}$$

$$K_{cr} = 12\sigma_{cr} \Big/ \left[\frac{\pi^2 E}{1-\nu^2}\left(\frac{t}{b}\right)^2\right] \tag{5.2b}$$

$$K_u = 12\sigma_u \Big/ \left[\frac{\pi^2 E}{(1-\nu^2)}\left(\frac{t}{b}\right)^2\right] \tag{5.2c}$$

$$K_A = 12\sigma_A \Big/ \left[\frac{\pi^2 E}{(1-\nu^2)}\left(\frac{t}{b}\right)^2\right] \tag{5.2d}$$

where

σ_c = any arbitrary vertical compressive stress

σ_{cr} = the vertical compressive stress at buckling

σ_u = the vertical compressive stress at ultimate load

σ_A = the vertical compressive stress calculated from the AISC specification.

These stresses are calculated by summing the loads over the test panel and dividing by the area of the compression edge of the web in the panel. It can be seen that K_{cr} in Eq. 5.2b is equal to the buckling coefficient for rectangular plates k.

5.3 Presentation and Comparison of AISC Specification and Buckling Loads

In the AISC specification, K_A is given by the following formulas:

top edge fixed

$$K_A = 5.5 + 4/(\alpha)^2 \qquad \alpha < 1 \qquad (5.3a)$$

$$K_A = (5.5 + 4/\alpha^2)1/\alpha \qquad \alpha > 1 \qquad (5.3b)$$

top edge simply supported

$$K_A = 2 + 4/\alpha^2 \qquad \alpha < 1 \qquad (5.4a)$$

$$K_A = (2 + 4/\alpha^2)1/\alpha \qquad \alpha > 1 \qquad (5.4b)$$

These values of K_A were obtained by multiplying the allowable vertical stress given by formulas 15 and 16 of the AISC Specification by the built-in safety factor (equal to 2.6) and dividing the result by the factor $\frac{\pi^2 E}{12(1-\nu^2)} \cdot \left(\frac{t}{b}\right)^2$. Notice that these equations is independent of z. Figures 39 and 40 show plots of K_A vs. α for the simply supported and fixed cases, respectively. Also shown are plots of K_{cr} for z = 0 given by the buckling theory. Since the AISC specification is based on a simplified buckling model of a plate, there should be some correlation between the two. For the simply supported case, the correlation is reasonably good but for the fixed case the difference is more significant. In Fig. 40, K_{cr} for z = 3 is also plotted. Here, the K values given by the theory are much lower than K_A for low values of α.

In Fig. 39, the values of K_{cr} obtained by Wilkesmann are also plotted for z = 0. The correlation between the Wilkesmann curve and that obtained from the computer program is reasonably good.

Figures 41 and 42 show the K_{cr} values obtained for the edge loading in Fig. 2 from the computer program. It can be seen here also that for low α values K_{cr} drops drastically as z increases. From these plots and that in Fig. 40, it can be seen that the simplified theory on which the AISC specification is based is not adequate when the panel is subjected to high bending stresses.

5.4 Comparison of Test Results With Theory and the AISC Specification

The primary purpose of the test series was to see what relation existed between K_u and K_{cr}. The test results will now be compared with the AISC specifications and the buckling theory for Case 2 (Art. 3.7), and an empirical relation between K_u and K_{cr} given. Table 3 gives the K_u values for each test panel. Notice that as expected, the K_u values decrease with increasing z. Table 3 also gives the ratios of K_u/K_{cr} and K_u/K_A for the tests. The ratios of K_u/K_{cr} show considerable post-buckling strength, as expected. Also, the ratios of K_u/K_{cr} are approximately constant, thus indicating that a relation does exist between the ultimate and buckling loads. It can be seen that the ratios of K_u/K_A decrease with increasing z, thus again showing the inadequacy of the AISC specification to predict the true behavior.

From the discussion above, the following conclusions can be drawn:

1. The effect of bending must be taken into account.
2. There is a considerable amount of post-buckling strength, and buckling does not mean failure.
3. Buckling theory does appear to predict the variation of the ultimate load with z.

There is also a slight reduction of K_u/K_{cr} with α. It is shown in Fig. 43 that the quantity $\sqrt{\alpha}\ K_u/K_{cr}$ is essentially a constant for all the tests. Thus, the post buckling strength appears to vary inversely with the square root of α. On the basis of the plot in Fig. 43 it may be concluded that the ultimate strength can be given conservatively by:

$$K_u = \frac{3.0}{\sqrt{\alpha}} K_{cr} \qquad (5.5)$$

This empirical relation should be limited to the range of $0 \leq z \leq 4.5$ and $0.8 \leq \alpha \leq 1.5$.

5.5 Behavior of Web

A secondary purpose of the tests was to attempt to verify the buckling loads given by the computer program, and in so doing, to determine what the actual boundary conditions of the web plate were. A mathematical theory for determining buckling loads on uniformly compressed rectangular plates from tests was proposed by Yoshiki and Fujita.[9] The buckling loads is determined by plotting load vs. the square of the lateral deflection. The second part of the curve is supposed to be straight, and the

buckling load is determined by extending the straight line back to the P axis, as shown in Fig. 44. The load-deflection relationships from the current test series did not lend themselves readily to such a construction because of large initial imperfections in the web plate. These large initial deflections apparently did not significantly affect the ultimate load because they were still small compared with the final deflections.

It was noted that in some of the tests, the vertical deflection remained linear up through the ultimate load, and returned very close to zero upon removal of the loads. This means that a failure of a loaded panel had little effect on the overall general behavior of the girder. Moreover, the panel which had been failed did carry the loads required of it when a neighboring panel was tested. The compression flange of a previously tested panel did not show any tendency to buckle into the web, even under high bending stresses. However, if the panel had been allowed to deform excessively during the test, the damage might have had an adverse effect on the general behavior of the girder. Also, a web failure under vertical compressive load could take place even if the remainder of the girder was elastic. This situation can become very critical for girders made of high strength steels.

There was no additional strength left in the test panel after formation of the yield band. In test EG-2.3, when the load was kept on after the formation of the yield band, the panel simply crumpled. Thus, the formation of the yield band is the signal that the failure is about to take place. If upon formation of the yield band, some of the vertical compressive load were taken off, the girder could be subjected to increased loads outside the test panel. However, the load which was still on cannot exceed the ultimate load for the increased z that would result from the increased load outside the test panel.

5.6 Items Not Considered

In this test series, no consideration of the effect of the slenderness ratio was made. For smaller β ratios, the effect of the web instability is probably less critical, and it would have less tendency to control the design proportions of the web. One test at a lower slenderness ratio of 192 for z = 0 was performed at Lehigh in 1963, giving a value of 2.0 for K_u/K_{cr}. More tests should be conducted before any conclusions can be drawn with respect to the influence of β.

No consideration on the effect of the yield stress of the web was made in this test series since all of the test panels had the same σ_y. Since this failure mode is expected to be more critical for higher strength steels, Eq. 5.5 would be conservative. For lower yield stresses, Eq. 5.5 would not be a safe prediction of the ultimate load.

5.7 Future Work

First, a method for the ultimate strength analysis should be developed for rectangular plates. The present test results could be used to check the validity of such a method. The web plate deformation pattern can be used as a guideline in formulating such a theory since the location of the yield pattern is well defined and predictable.

Secondly, more tests should be run on high strength plate girders so that the effect of high z and different yield stress on K_u can be established. In any future tests, a stronger effort should be made to ensure that the yield stress of the flanges is equal to or greater than that of the web. Tests should also be conducted for different slenderness ratios. These tests would establish the variation of K_u with yield stress and the slenderness ratio, and more test points would be provided for comparison with the ultimate strength theory.

Thirdly, in future tests, it would be desirable to obtain more information about the strain distribution at the junction between the edge of the web and the top flange at working loads. Then, the results can be combined with existing fatigue studies to learn whether or not fatigue is a problem and how it can be taken into account.

6. SUMMARY AND CONCLUSIONS

The objective of this investigation was to determine the buckling characteristics and the ultimate strength of the web of plate girder panels subjected to vertical compressive load bearing through the compression flange between stiffeners combined with bending and shear on the panel.

A computer program was developed to determine the buckling loads of the web plate under vertical compression and bending using some simplifying assumptions with respect to the stress distribution. The results of this analysis are shown in Figs. 41 and 42.

Ten tests on three plate girders were conducted to determine the K_u value of the web plate when subjected to combined bending and vertical compressive load; and combined shear, bending and compressive load.

The test results showed that the ultimate load was between three and four times the buckling load, thus indicating a considerable post buckling strength. The ratio of K_u/K_{cr} was approximately constant for a given aspect ratio, and it varied inversely with the square root of the aspect ratio, α.

Failure of the test panel occurred before any other inelastic behavior in tests with low z, and it had little effect on the overall behavior of the girder except in tests where yielding took place in plate elements other than the web.

Web deflections were of the order of three to six times the plate thickness at ultimate load.

Failure was caused by the formation of a band of yielding across the web panel whose location varied only with α and not with load distribution.

7. ACKNOWLEDGEMENTS

This report was prepared in connection with a research project on plate girders conducted in the Department of Civil Engineering, Fritz Engineering Laboratory, Lehigh University, Bethlehem, Pennsylvania. Dr. Lynn S. Beedle is the Acting Head of the Department and Director of the Laboratory.

The work described here was sponsored by the American Institute of Steel Instruction. The authors wish to thank this organization and in particular, Messrs. T. R. Higgins and W. A. Milek for sponsoring this research.

Sincere appreciation is expressed for the able help of the Fritz Engineering Laboratory staff and technicians, and especially to James Dimitri for his help during the testing program. Also, sincere thanks goes to Sharon Gubich and J. M. Gera for their help with the drawings, R. N. Sopko for this help on the photographs and to Marilyn Courtright for her patience in typing the manuscript.

8. NOMENCLATURE

a	panel length
A,B,C,D	integration constants
A_w	area of web
b	panel depth
d_1	vertical distance between mesh points
d_2	horizontal distance between mesh points
E	modulus of elasticity
k	buckling coefficient
K, K_A, K_{cr}, K_u	stress parameters
L	length
m	index giving location of a mesh point in a column
n	index giving location of a mesh point in a row
N	normal
P	load
t	plate thickness
U,V	coefficient matrices generated from finite difference operators
w	lateral deflection; lateral deflection vector
W	distributed load
$\overline{X},\overline{Y}$	components of distributed edge forces per unit area
z	σ_b/σ_c, ratio of maximum compressive bending stress to the vertical compressive edge stress

α	aspect ratio a/b
β	slenderness ratio b/t
γ	d_2/d_1
δ	experimental lateral deflection
Δ	experimental vertical deflection
ϵ	strain
ν	Poisson's ratio
σ	normal stress
σ_A	allowable vertical compressive stress given by AISC specification
σ_b	maximum compressive bending stress
σ_c	vertical compressive stress
σ_{cr}	buckling vertical compressive stress
σ_u	ultimate vertical compressive stress; ultimate stress
σ_x	normal stress in x direction
σ_y	normal stress in y direction; yield stress
τ	shear stress
τ_{xy}	shear stress on differential element
ϕ	stress function

9. TABLES AND FIGURES

Table 1 Summary of Plate Girder Dimensions

Girder	No. of Panels	Tests	α	Test Panel Length inches	Girder Length feet	Thickness of Web, inches	Depth inches
EG-1	3	4	0.8	28	30	0.1205	36
EG-2	3	4	1.2	43	30	0.1224	36
EG-3	2	2	1.6	57	25	0.1216	36

Table 2 Material Properties

Girder	Component	σ_y ksi 0.2% Offset	σ_y 0.5% Strain	σ_y ksi	% Elong.	% Area Reduction	Strain Hardening Modulus ksi
EG-1	Top Flange	34.2	--	62.5	35.0	61.1	825
EG-1	Bottom Flange	33.3	--	63.1	37.1	61.8	527
EG-1	Web-Horizontal Direction	42.4	44.3	68.1	27.6	49.3	534
EG-1	Web-Vertical Direction	44.4	45.7	72.7	30.0	52.2	718
EG-2	Top Flange	36.7	--	65.0	38.4	58.2	827
EG-2	Bottom Flange	36.1	--	65.4	36.2	57.1	488
EG-2	Web-Deflection Direction	43.2	43.9	69.6	27.0	52.0	729
EG-2	Web-Vertical Direction	43.6	44.9	70.9	25.6	48.1	483
EG-3	Top Flange	33.3	--	63.4	38.6	60.3	726
EG-3	Bottom Flange	34.9	--	65.1	35.6	59.1	703
EG-3	Web-Horizontal Direction	43.4	44.1	70.3	28.3	54.5	559
EG-3	Web-Vertical Direction	43.5	43.8	69.8	23.3	49.6	597

Table 3 Test Results and Comparisons

α	Z	Test No.	P_u Kips	K_u	K_{cr}	K_A	K_u/K_{cr}	$(K_u/K_{cr})\sqrt{\alpha}$	K_u/K_A
0.8	0.82	EG-1.1	49.6	48.4	12.0	11.8	4.0	3.6	4.1
0.8	3.82	EG-1.2	28.0	27.3	6.9	11.8	3.9	3.5	2.3
0.8	2.44	EG-1.3	36.5	35.6	8.6	11.8	4.1	3.7	3.0
0.8	1.1	EG-1.4	41.0	39.9	11.2	11.8	3.6	3.2	3.4
1.2	4.5	EG-2.1	30.0	19.0	6.1	6.9	3.1	3.4	2.7
1.2	2.4	EG-2.2	57.0	36.0	7.5	6.9	4.8	5.25	5.21*
1.2	1.37	EG-2.3	46.0	29.0	8.2	6.9	3.5	3.8	4.2
1.2	1.22	EG-2.4	43.5	27.4	8.2	6.9	3.3	3.6	3.9
1.6	1.90	EG-3.1	45.0	21.5	7.0	4.8	3.1	3.9	4.5
1.6	3.19	EG-3.2	38.0	18.2	6.5	4.8	2.8	3.5	3.8

* An excessively high ultimate load in test EG-2.2 was caused by a wood loading beam which distributed some load to the stiffeners.

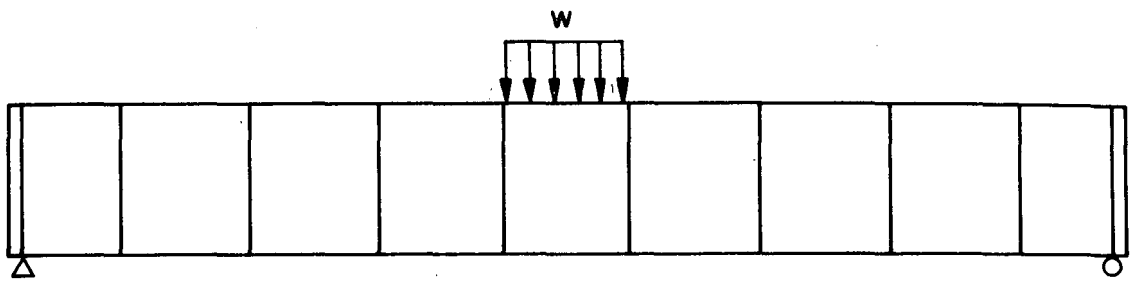

Fig. 1 Plate Girder Under Edge Comparison

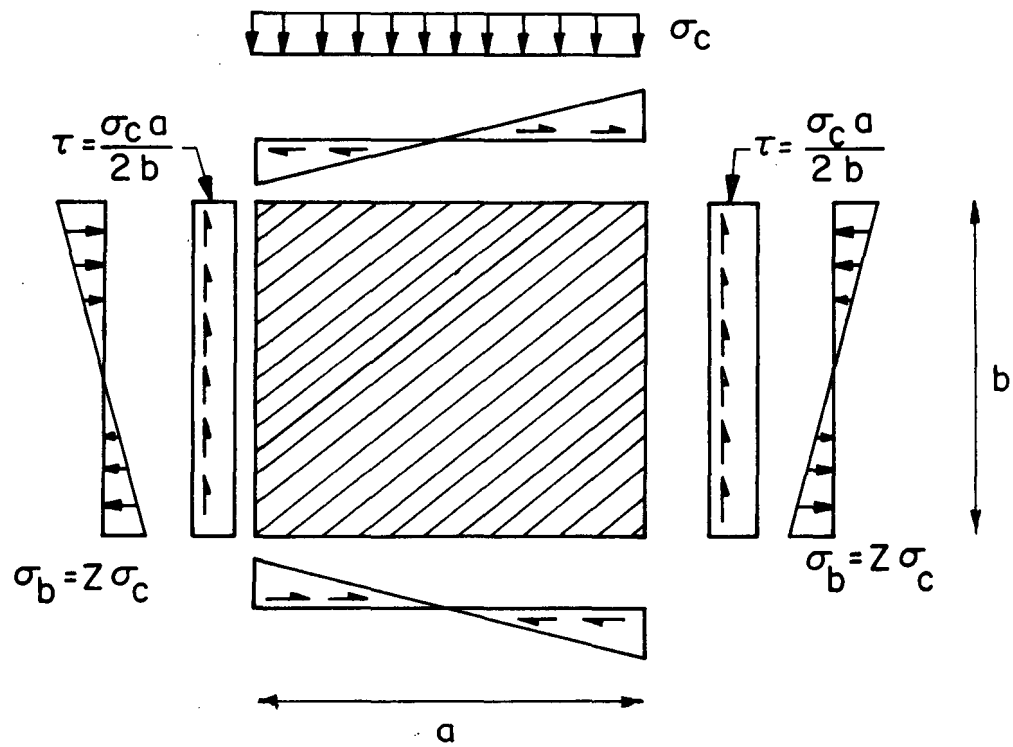

Fig. 2 Assumed Edge Loading for Panel Under Uniform Moment

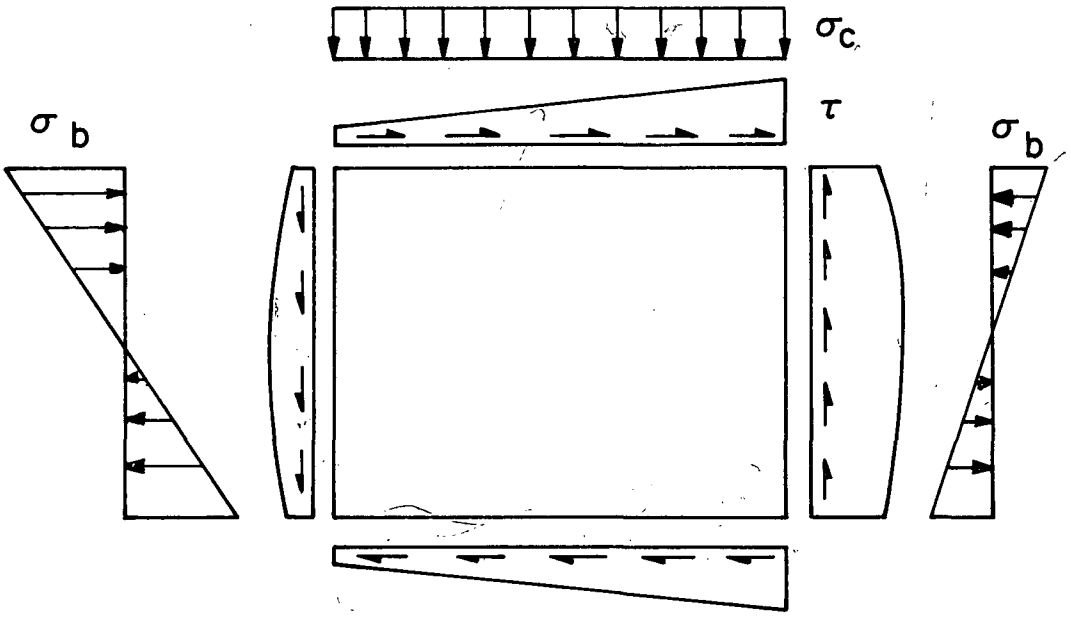

Fig. 3 Edge Loads for Panel Under Shear and Bending

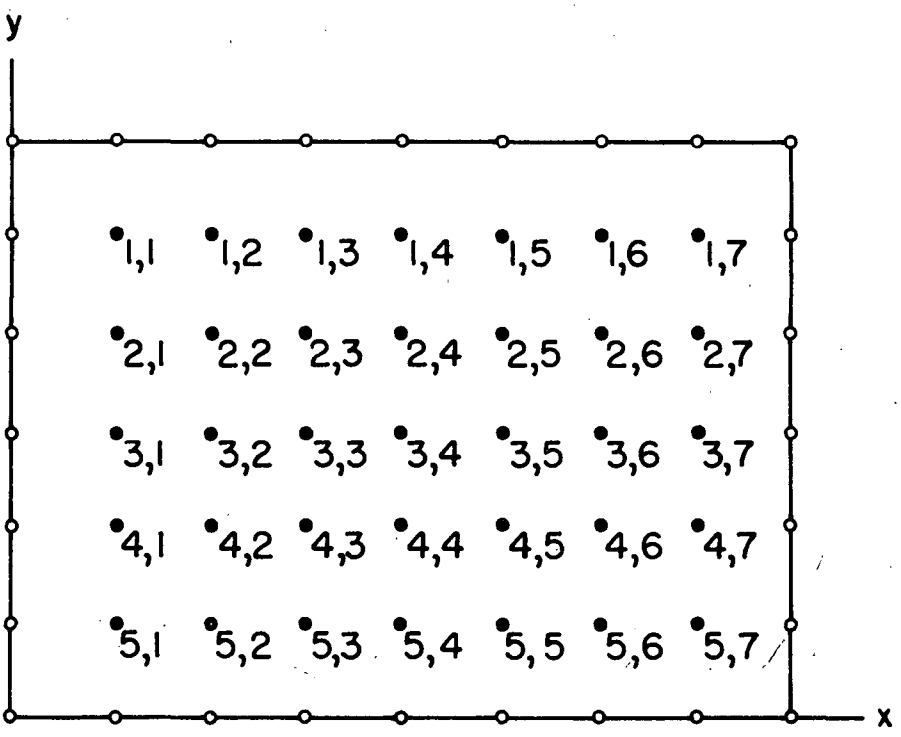

Fig. 4 Finite Difference Mesh Points

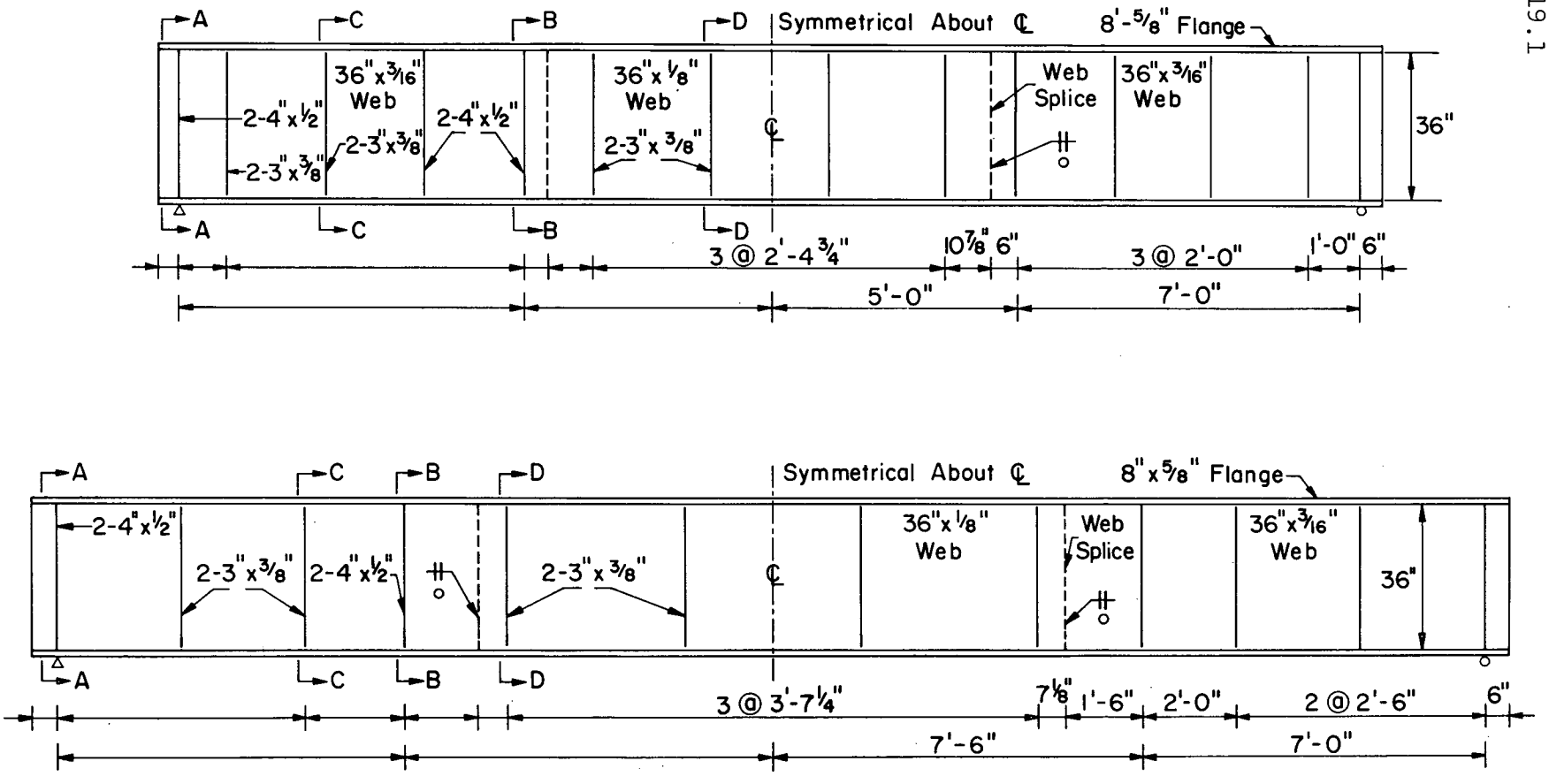

Fig. 5 Girders EG-1 and EG-2

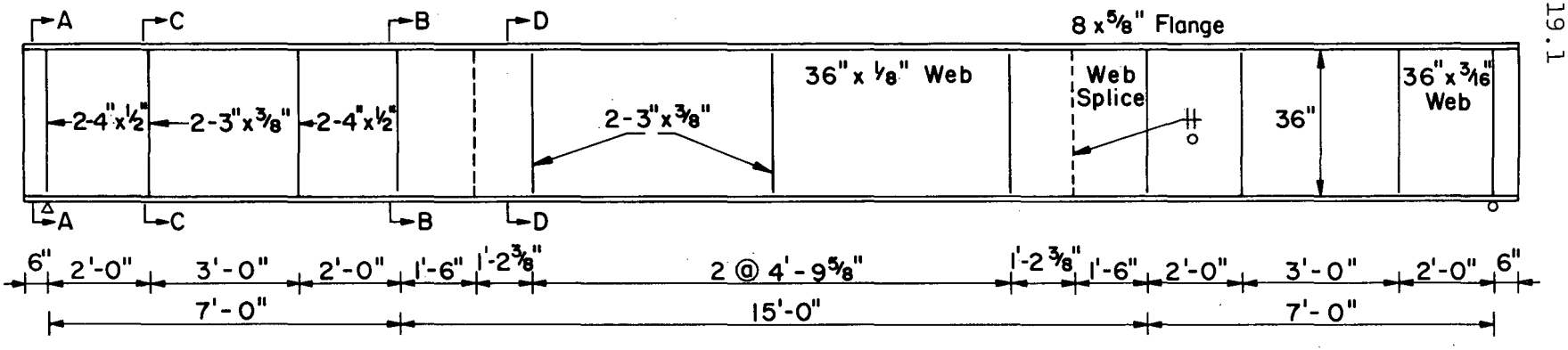

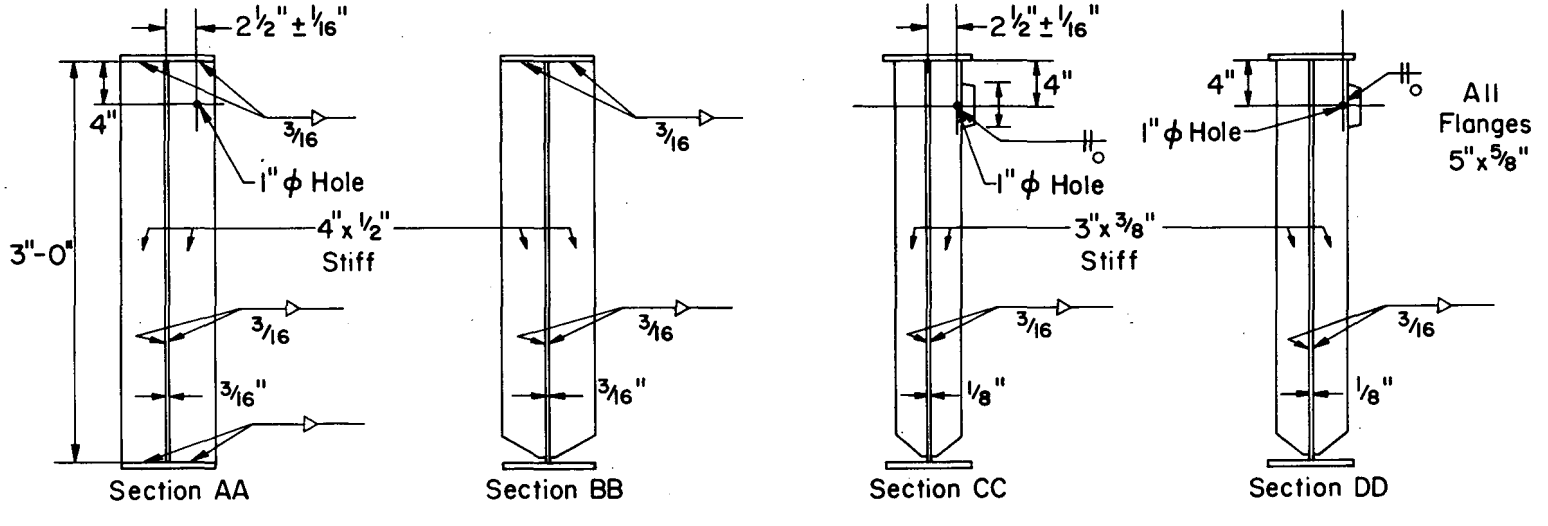

Fig. 6 Girder EG-3 and Sections AA, BB, CC, and DD for All Girders

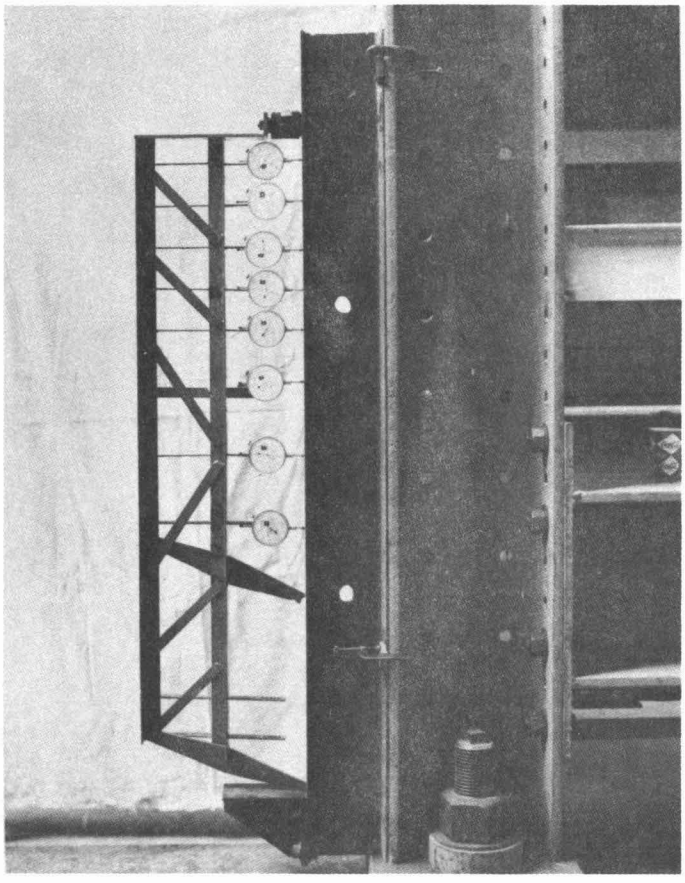

Fig. 7 Dial Rig for Lateral Deflection Measurement

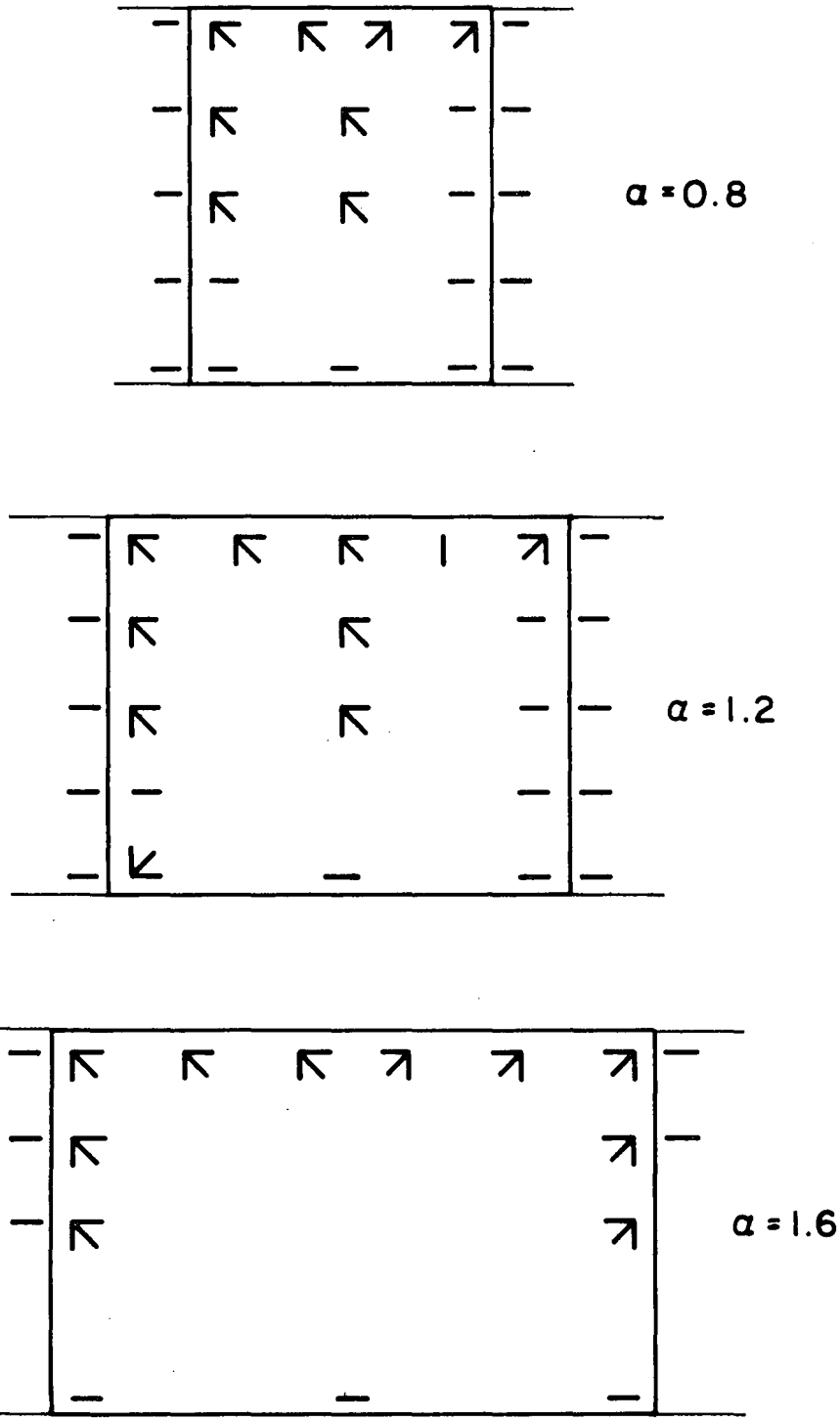

Fig. 8 Strain Gage Arrangement for Typical Test Panels

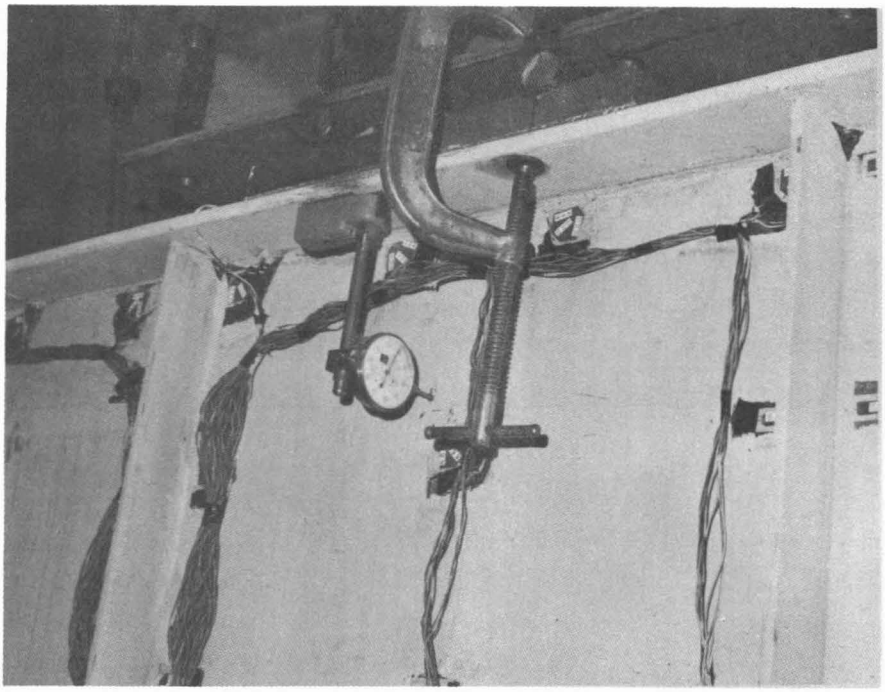

Fig. 9 Dial Gage for Lateral Deflection Measurement

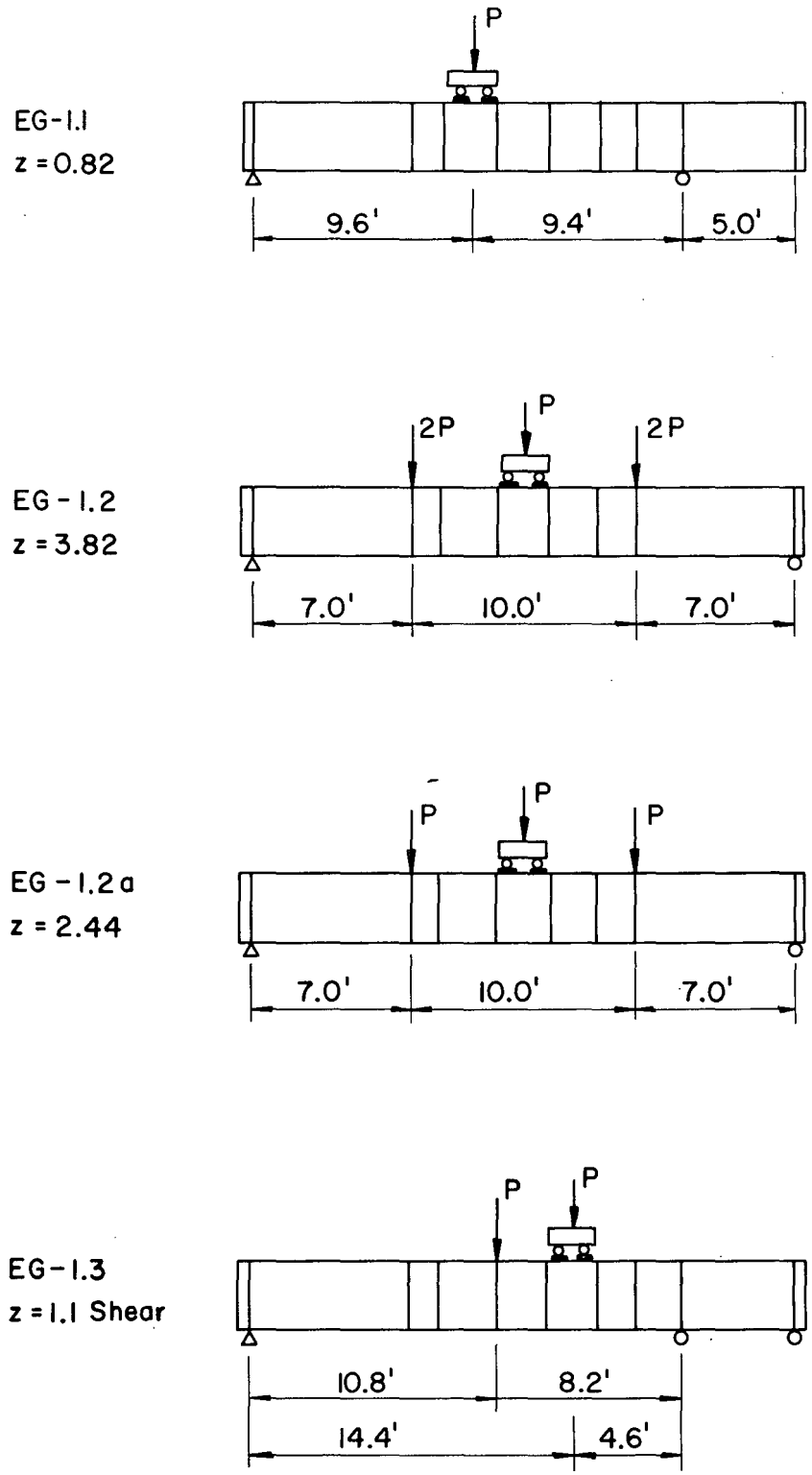

Fig. 10 Test Set-Ups for EG-1

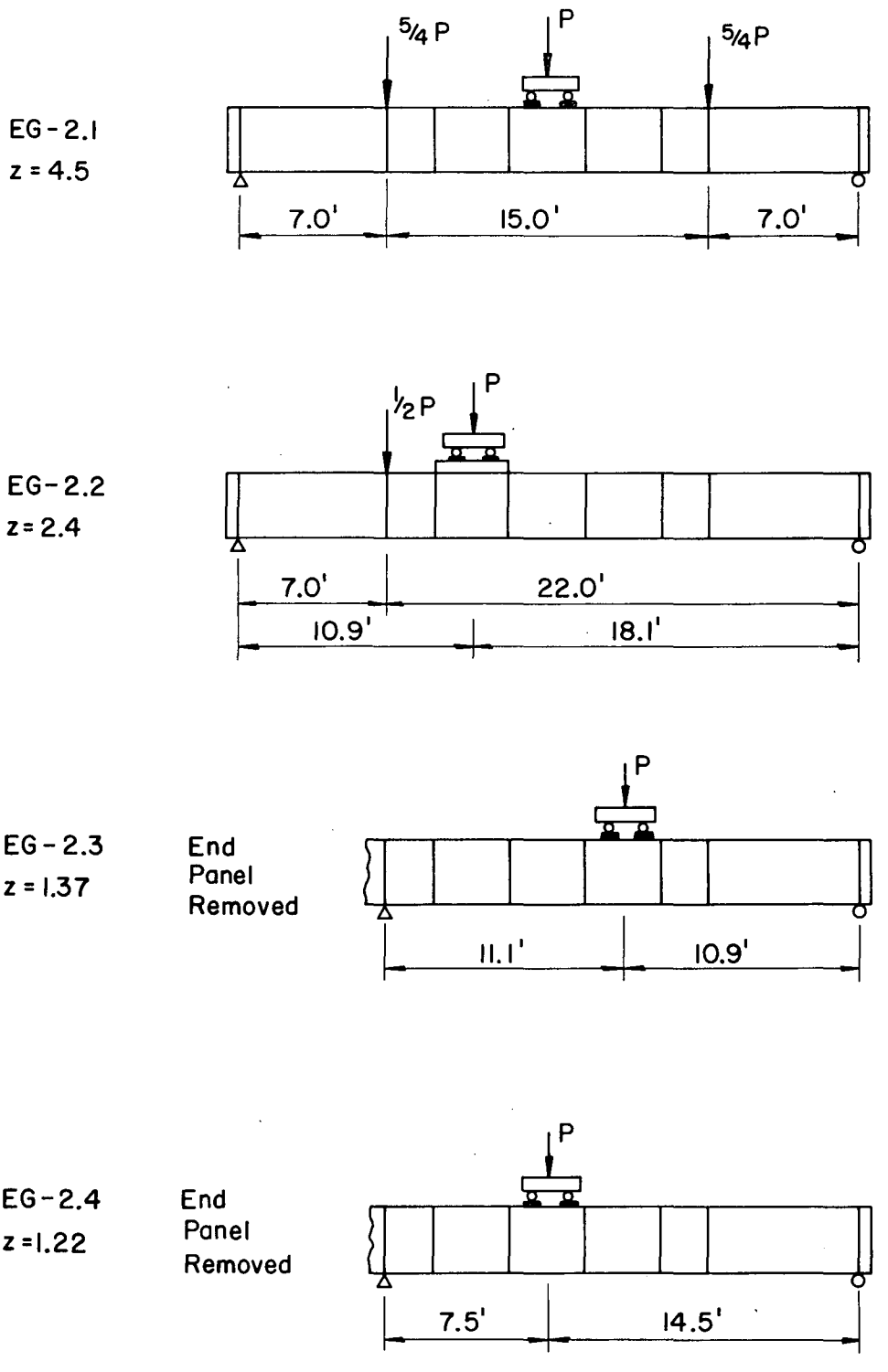

Fig. 11 Test Set-Ups for EG-2

EG - 3.1
z = 1.90

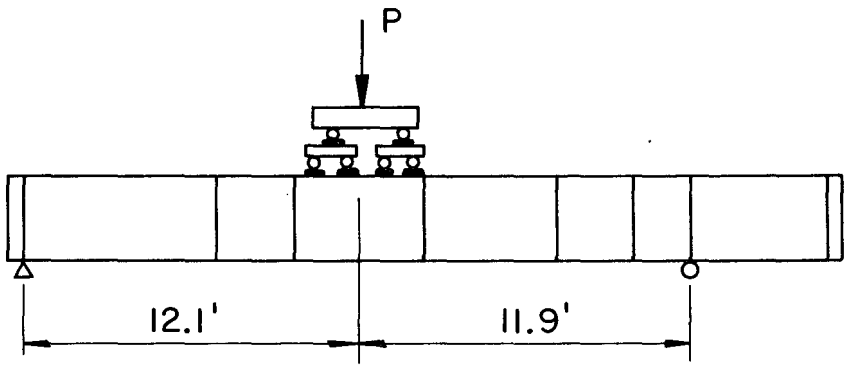

EG-3 2
z = 3.19
Shear

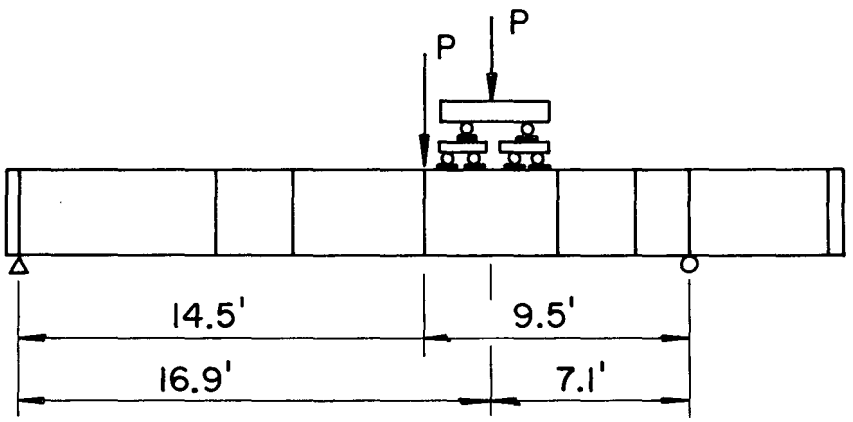

Fig. 12 Test Set-Ups for EG-3

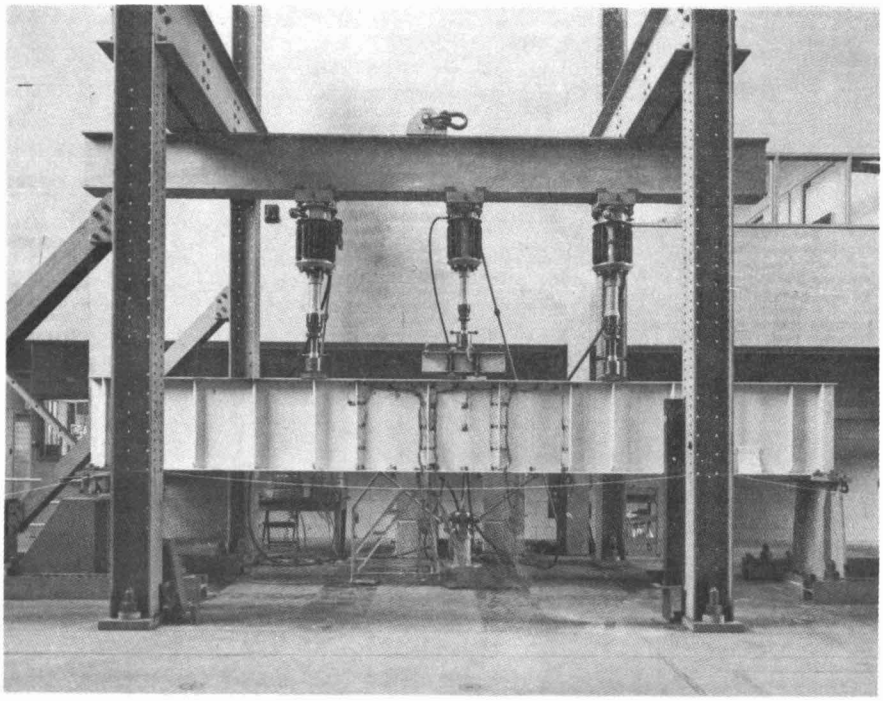

(a)

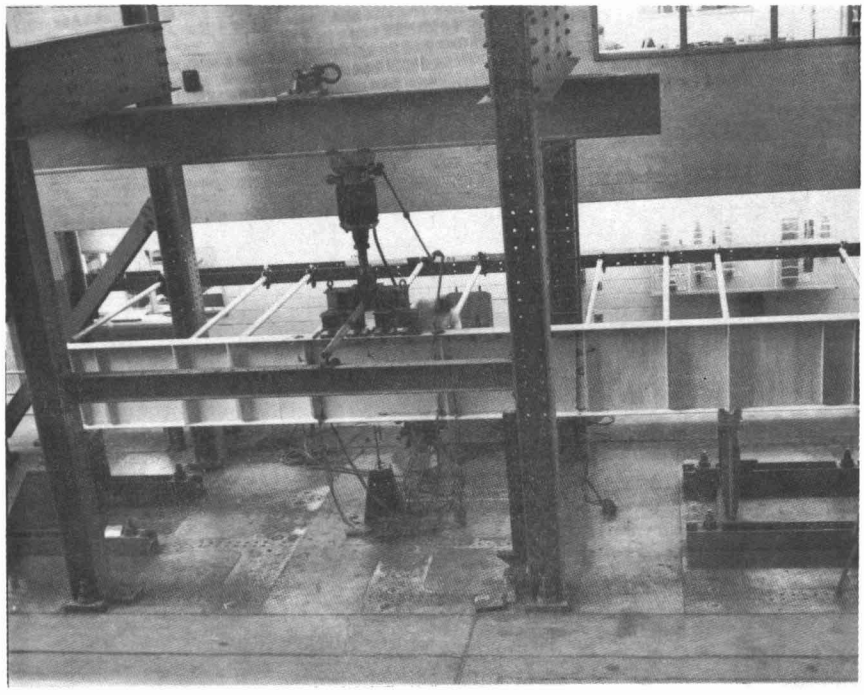

(b)

Fig. 13 Test Set-Ups for (a) EG1.2 and (b) EG-3.1

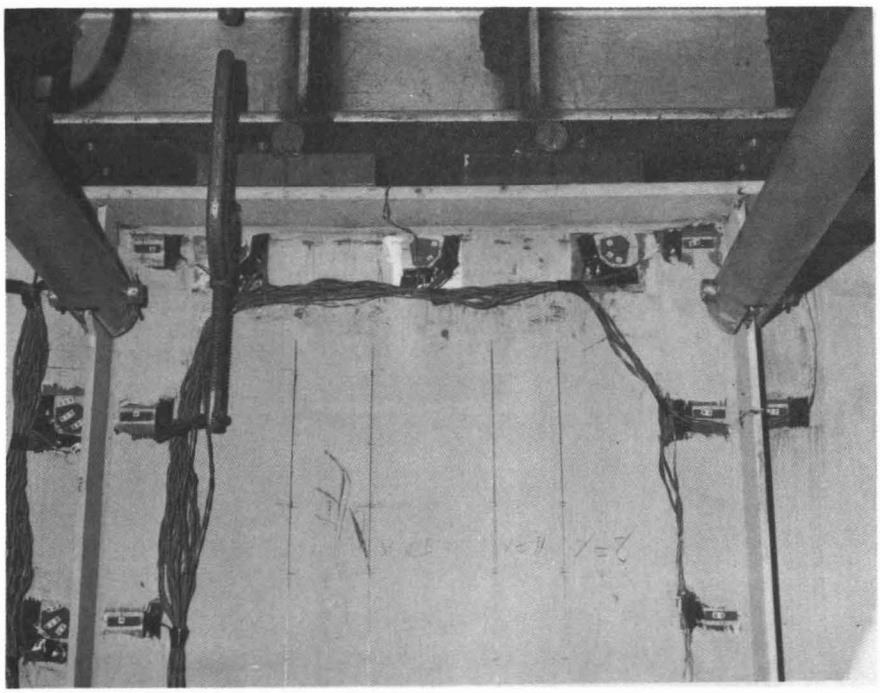

Fig. 14 Load Distribution Mechanism Over Test Panel EG-2.1

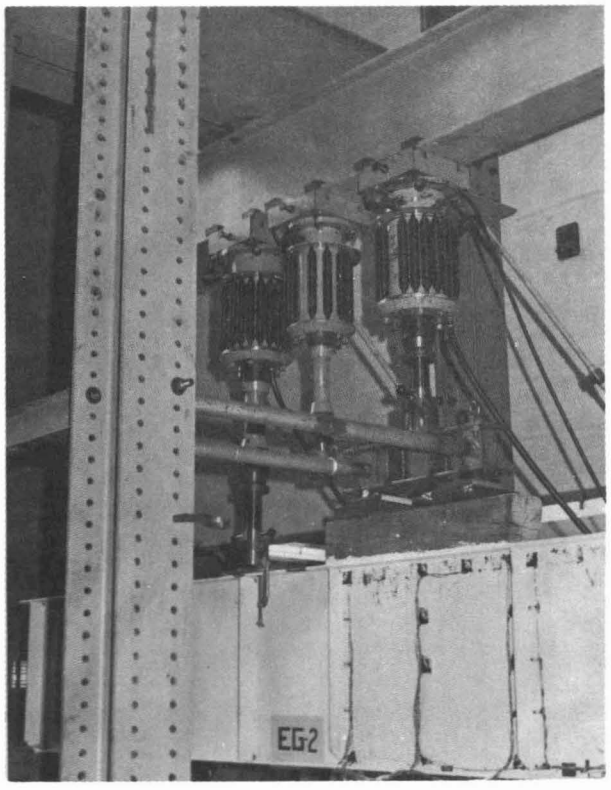

(a)

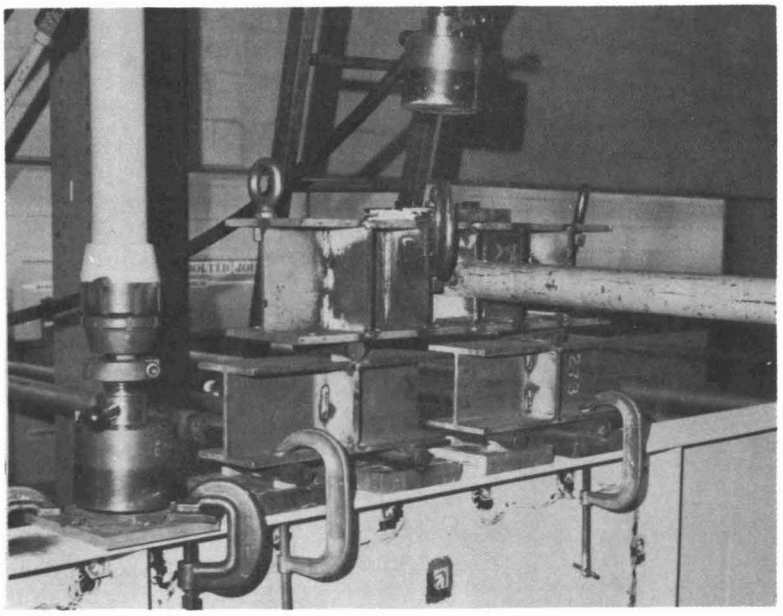

(b)

Fig. 15 Load Distributing Mechanism for EG-2.2 and EG-3.2

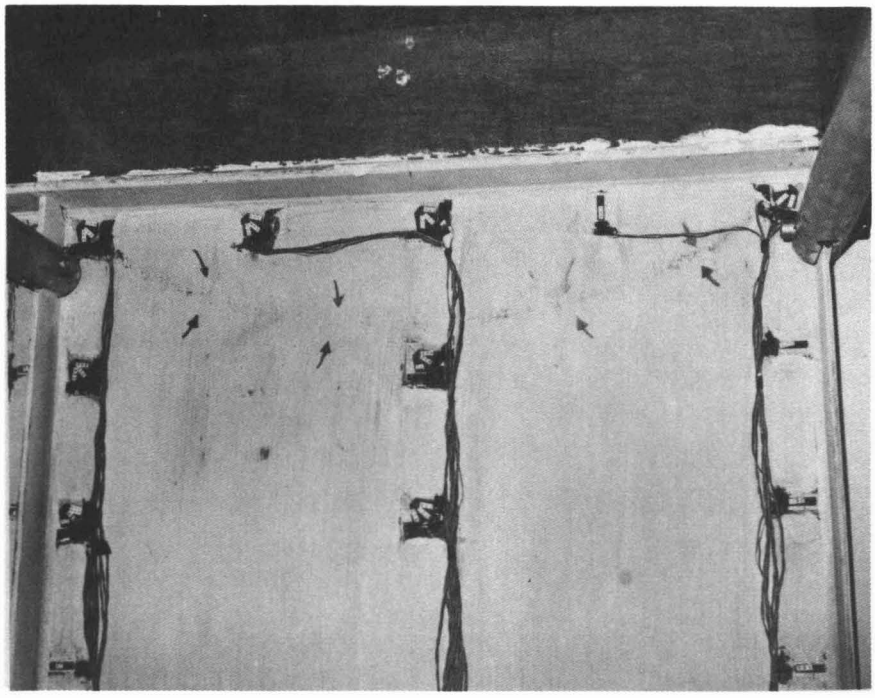

Fig. 16 Failure Panel Showing Yield Bend

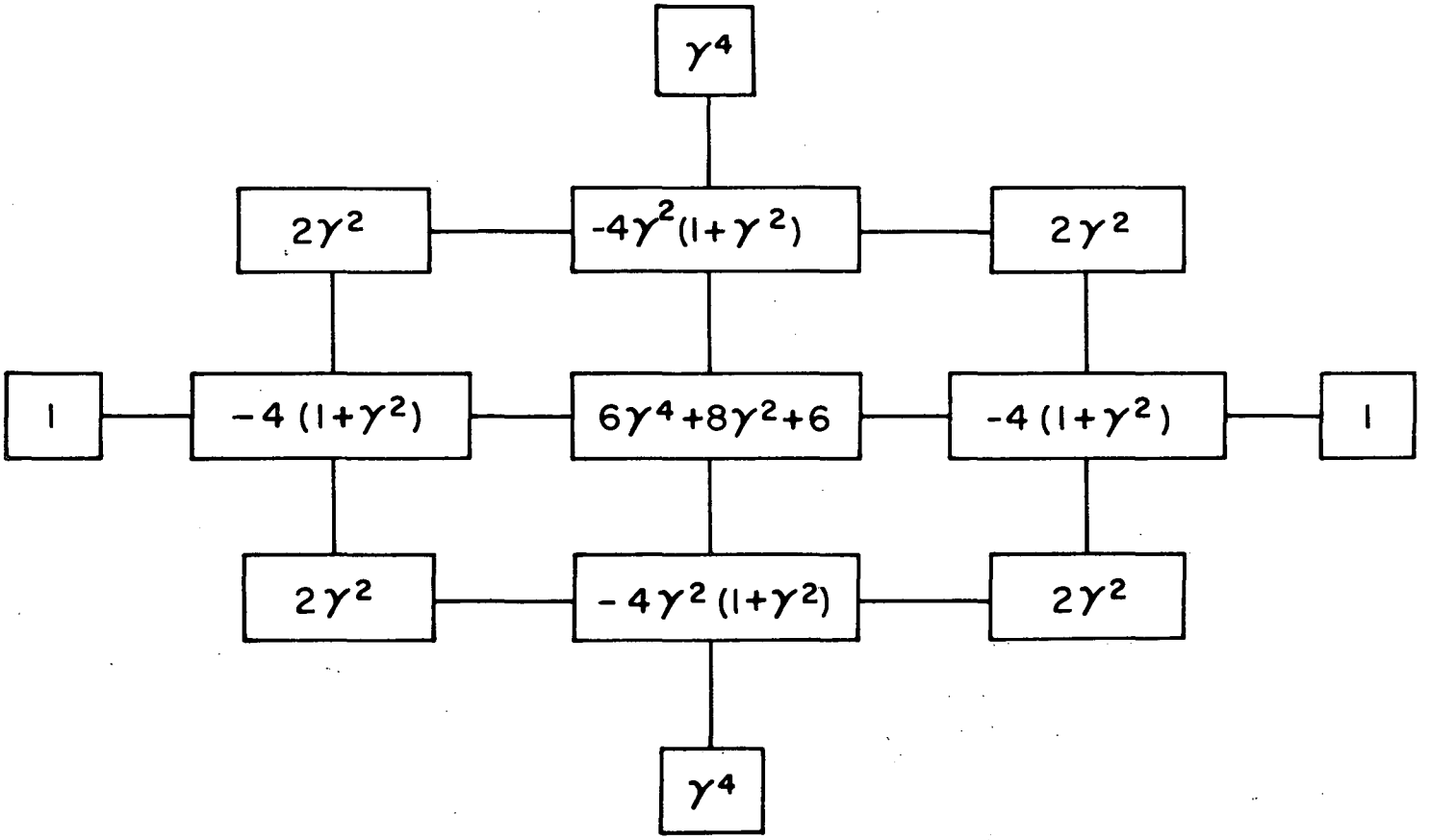

Fig. 17 Finite Difference Operator for $\nabla^4 \phi$

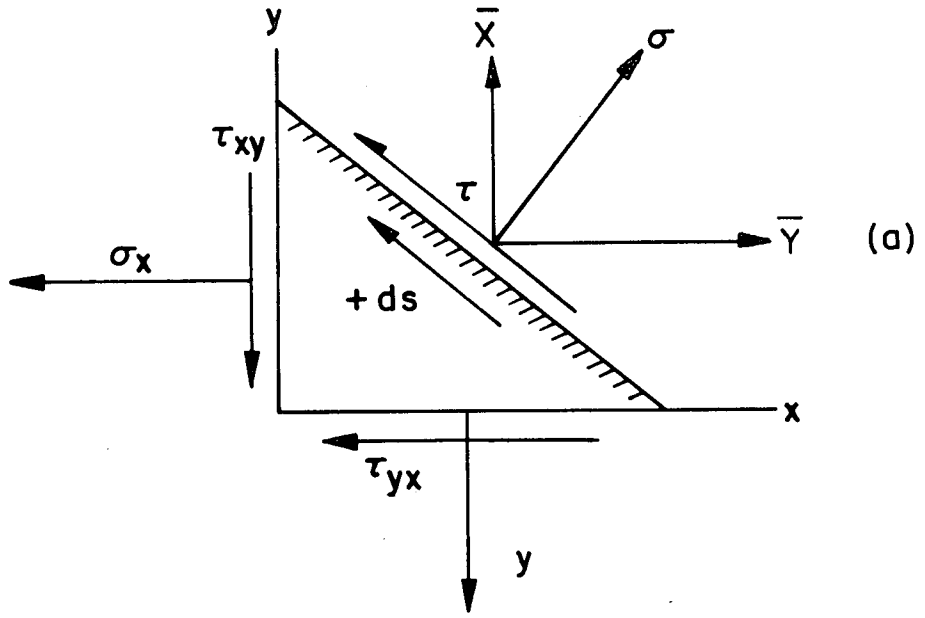

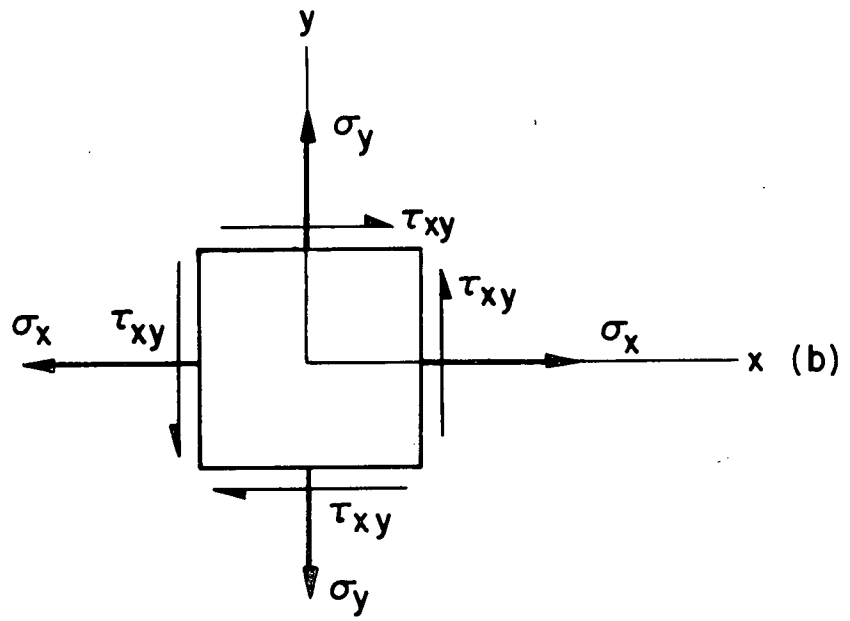

Fig. 18 Differential Elements

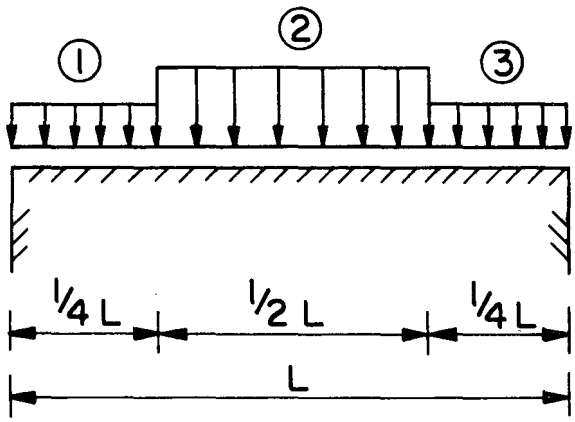

Fig. 19 Segments of Loading

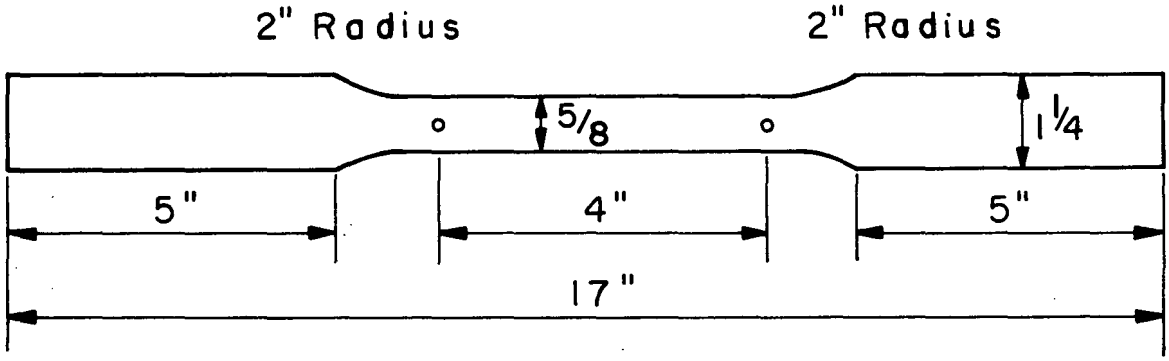

Fig. 20 Flange Tensile Specimen

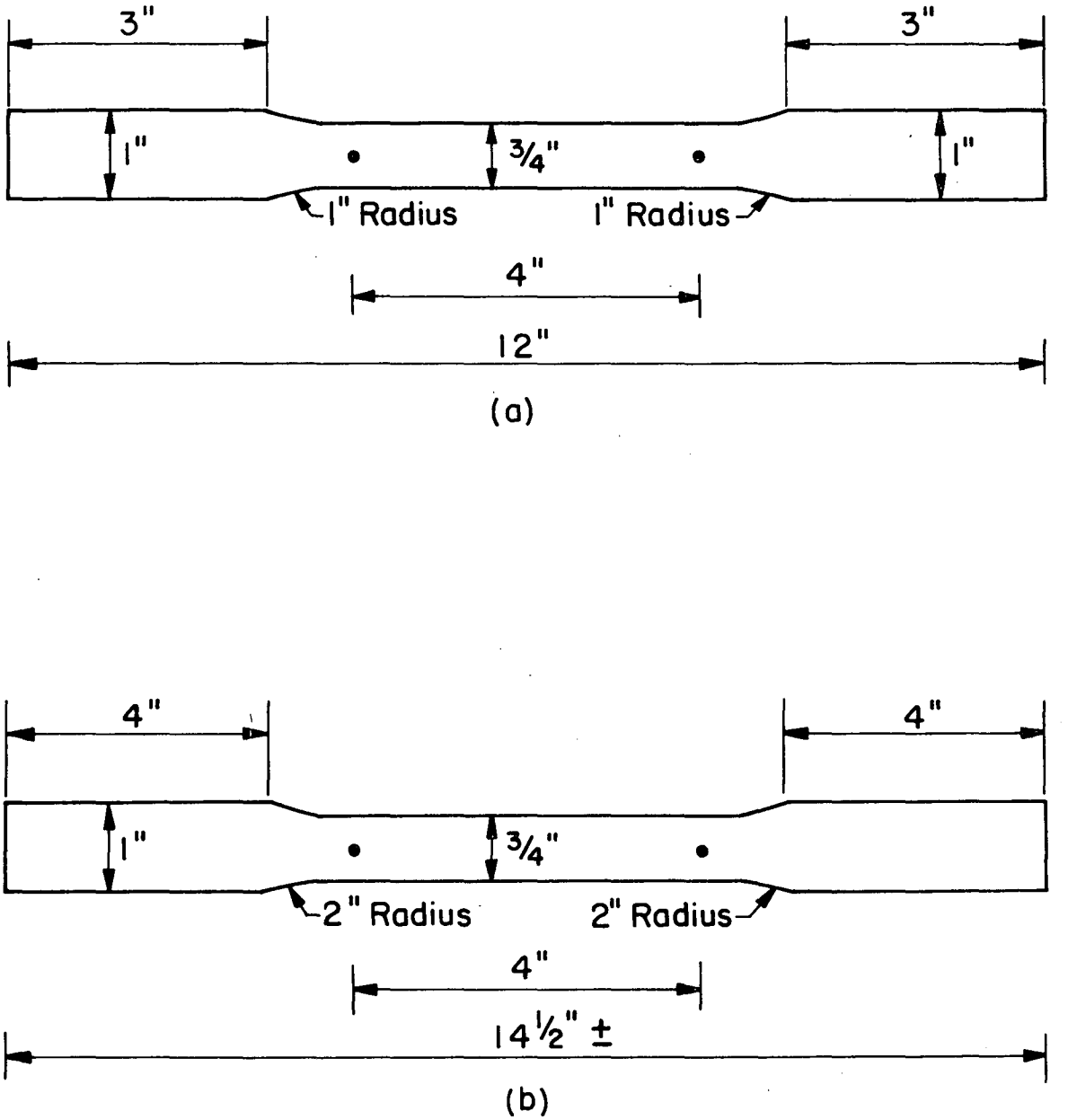

Fig. 21 Web Tensile Specimens

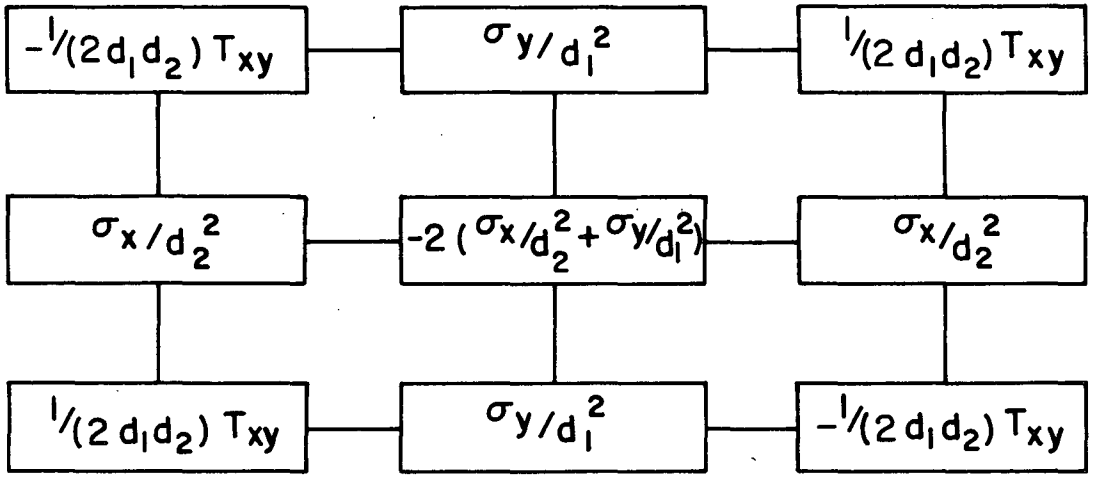

Fig. 22 Finite Difference Operator

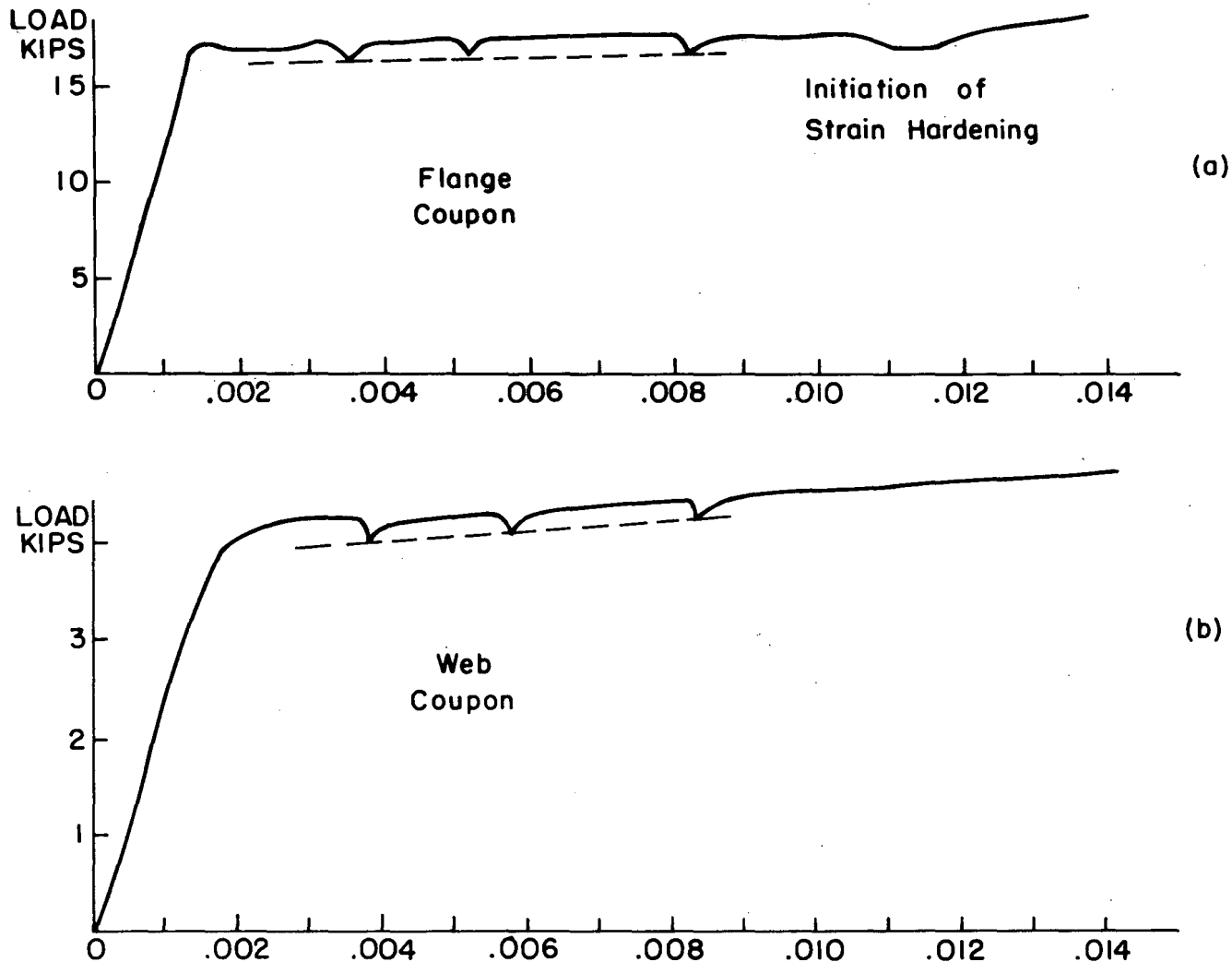

Fig. 23 Load-Strain Curves for Tensile Specimens

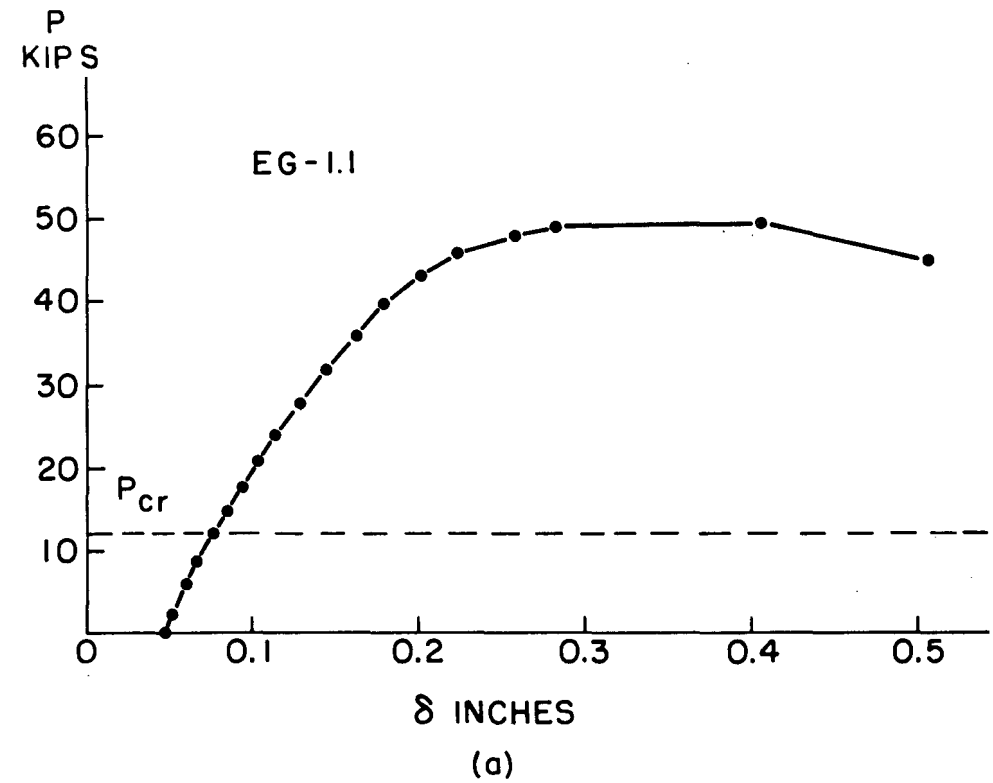

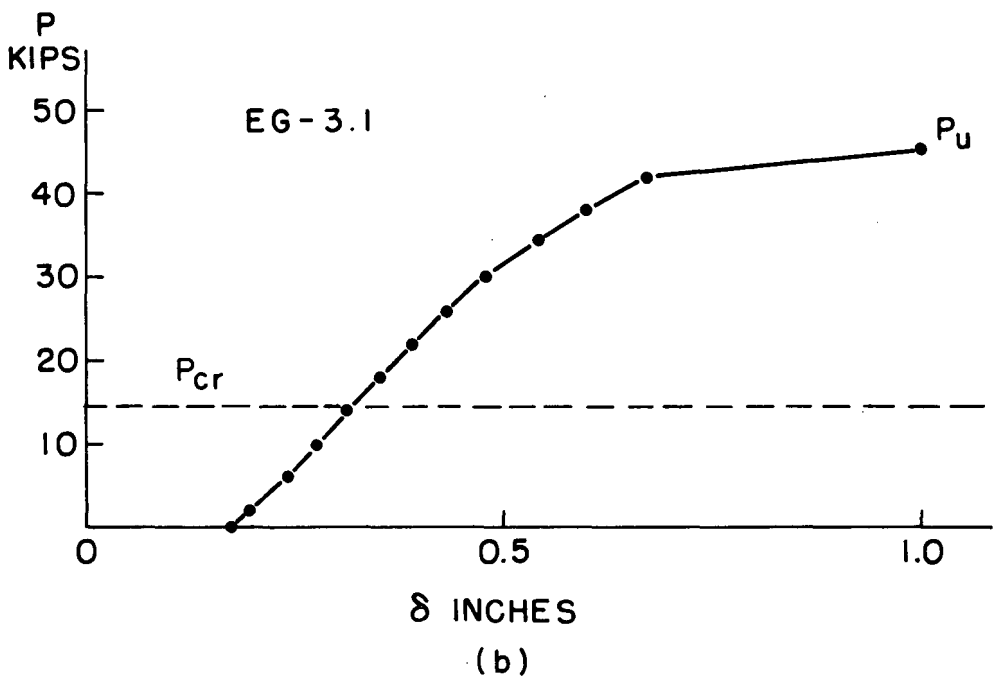

Fig. 24 Load Vs. Lateral Deflection Curves

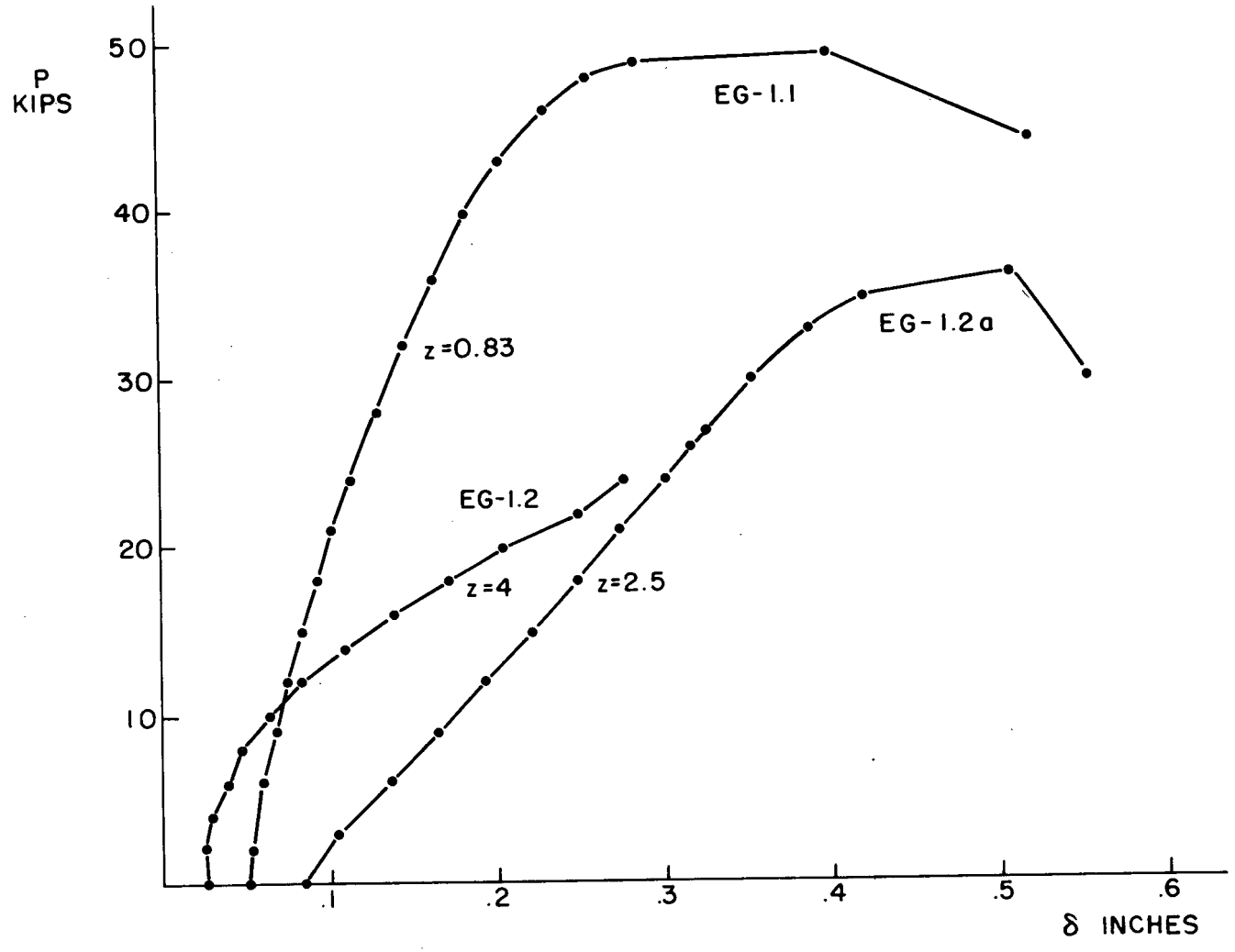

Fig. 25 Load Vs. Lateral Deflection Curves

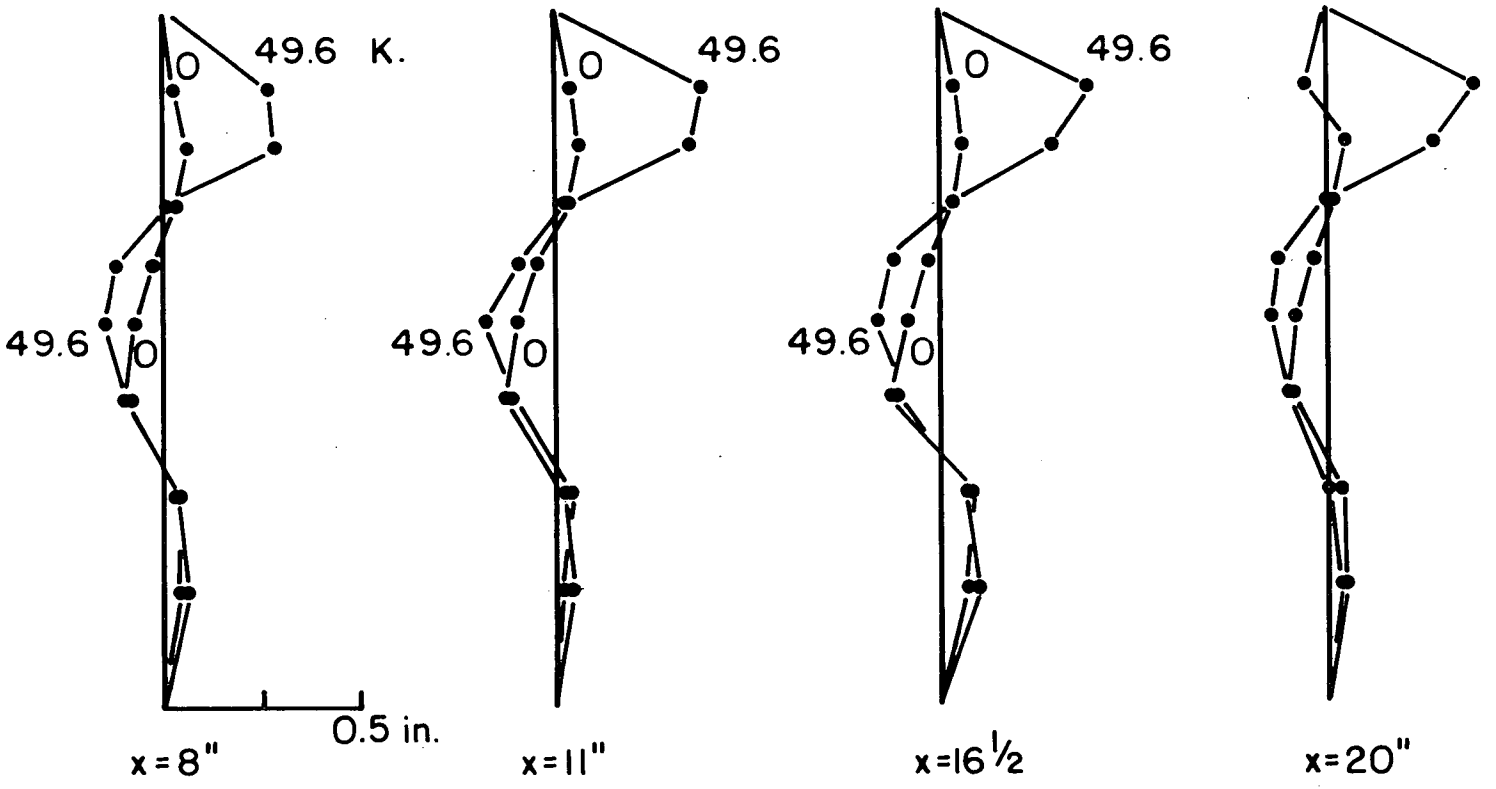

Fig. 26 Original and Final Lateral Deflection Patterns on Test Panel for EG-1.1

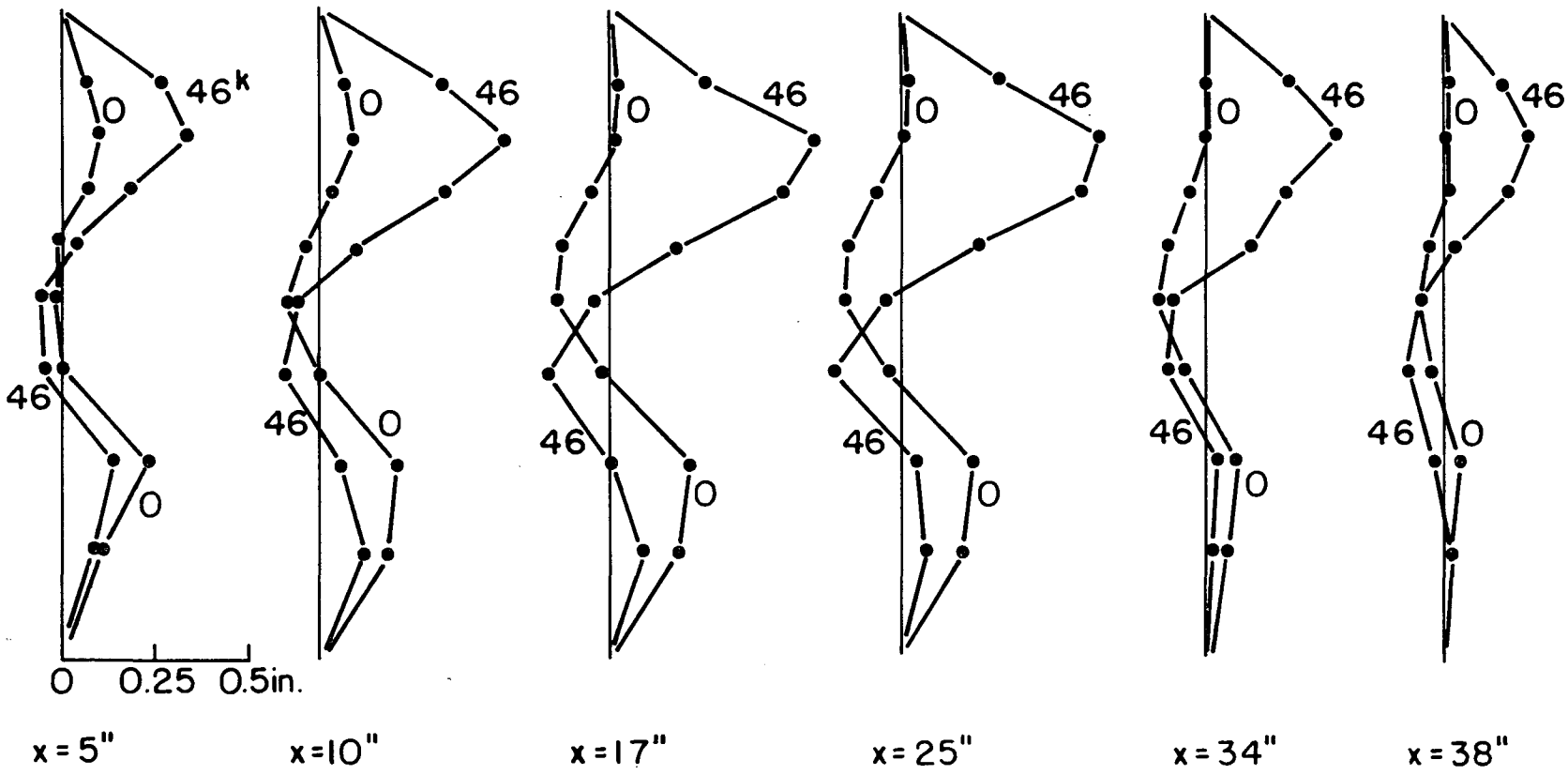

Fig. 27 Original and Final Lateral Deflection Pattern on Test Panel for EG-2.3

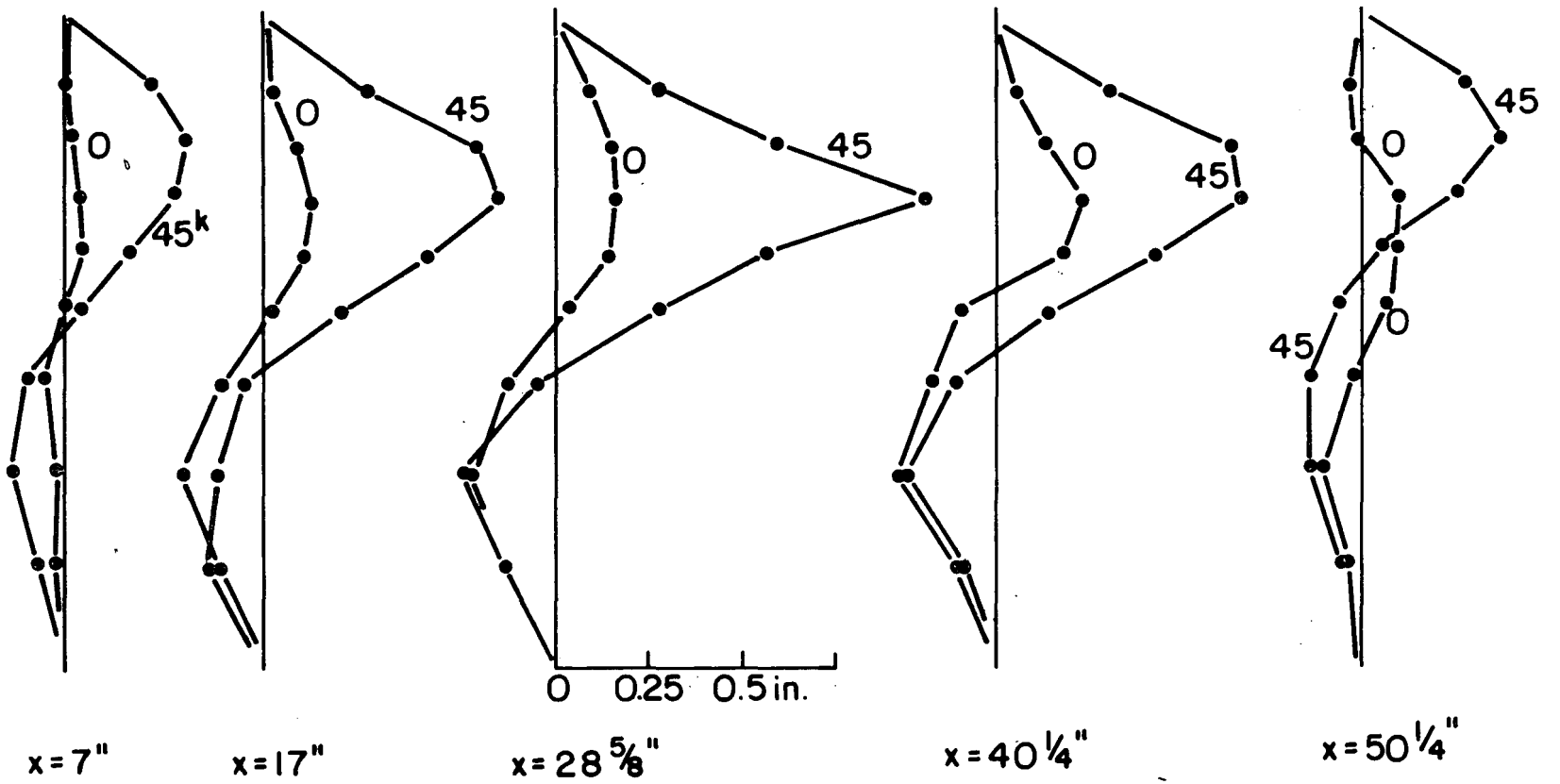

Fig. 28 Original and Final Lateral Deflection Pattern on Test Panel for EG-3.1

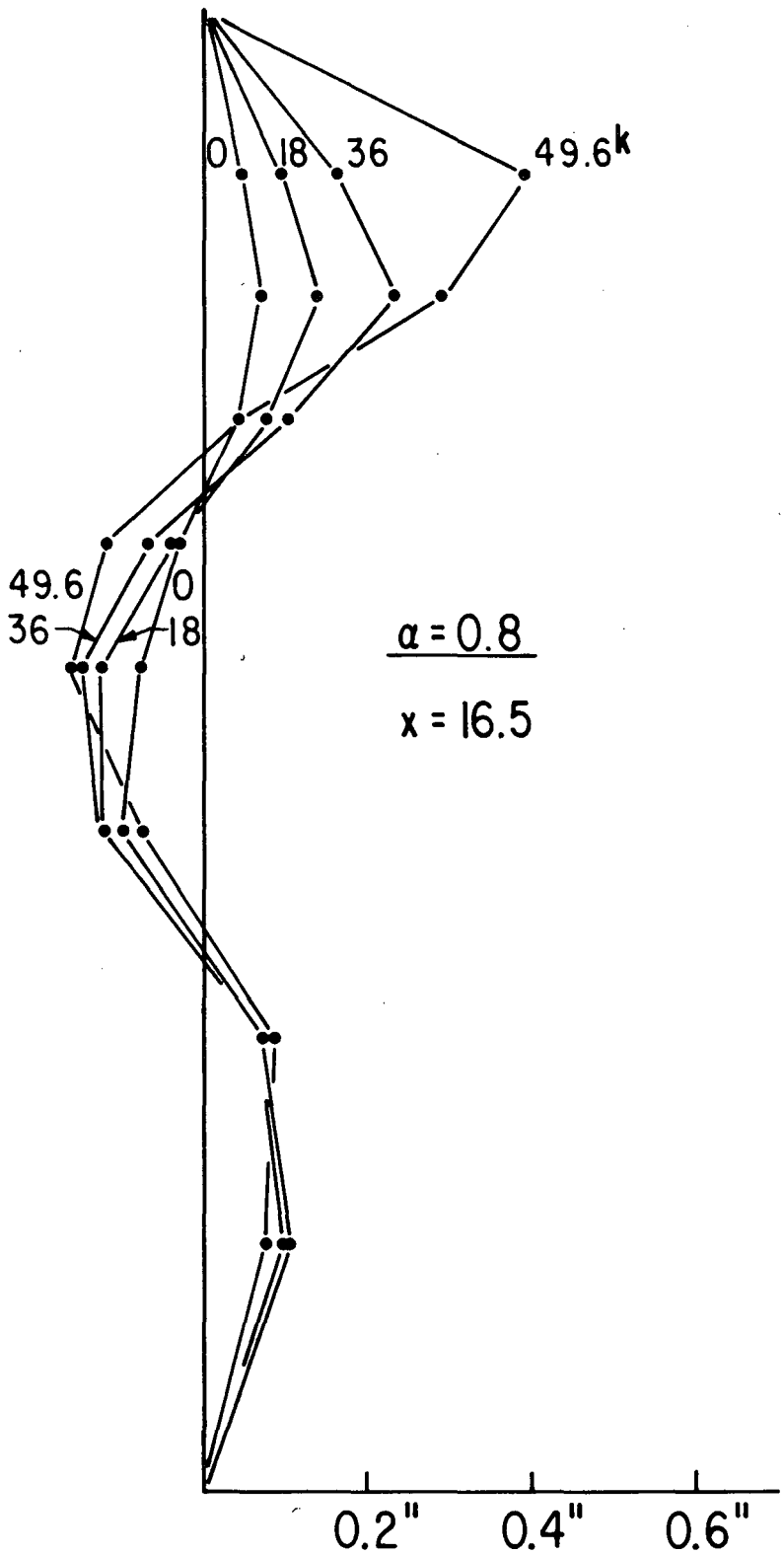

Fig. 29 Progress of Lateral Deflection Near Center of Test Panel, EG-1.1

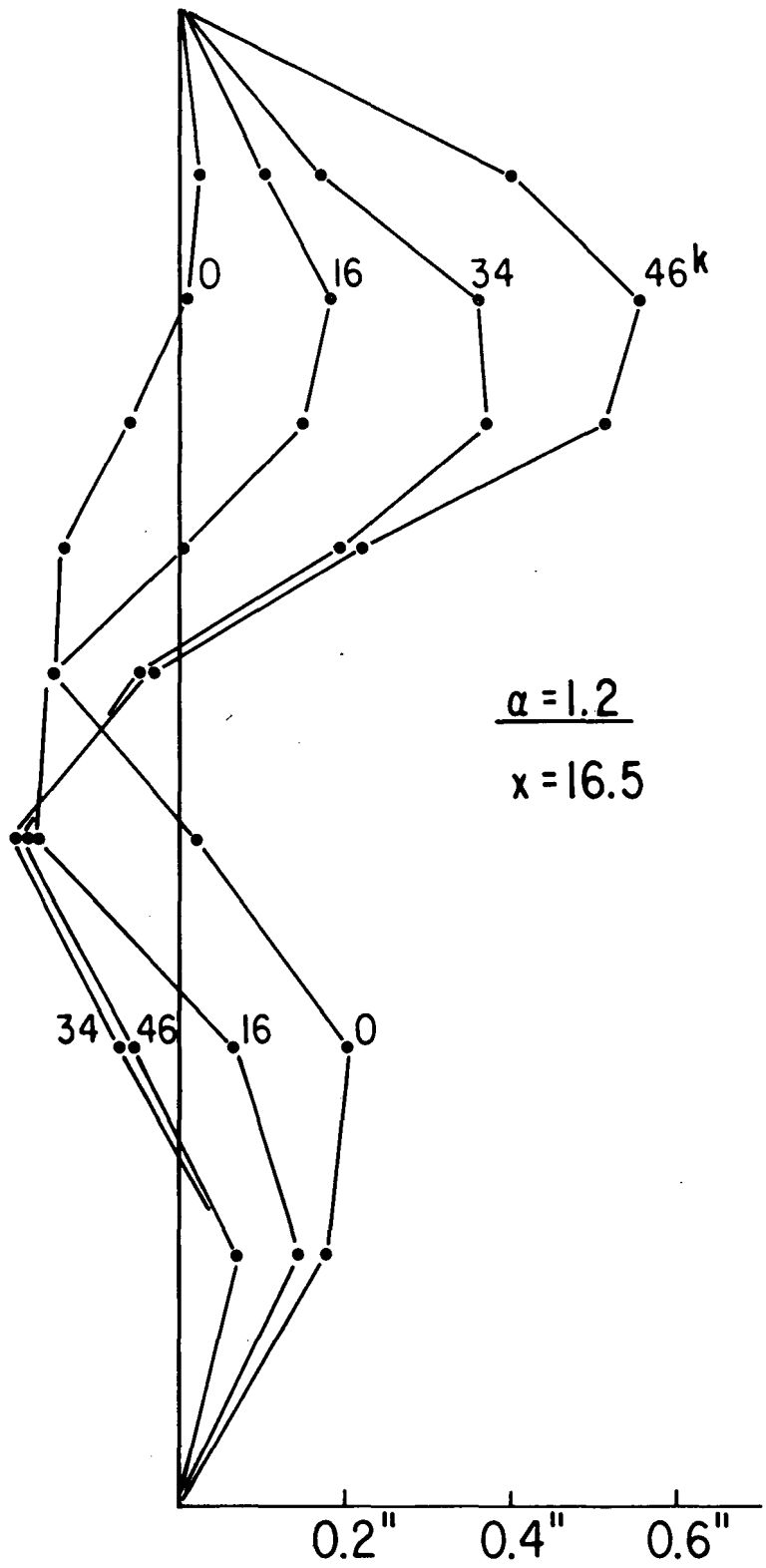

Fig. 30 Progress of Lateral Deflection Near Center of Test Panel, EG-2.3

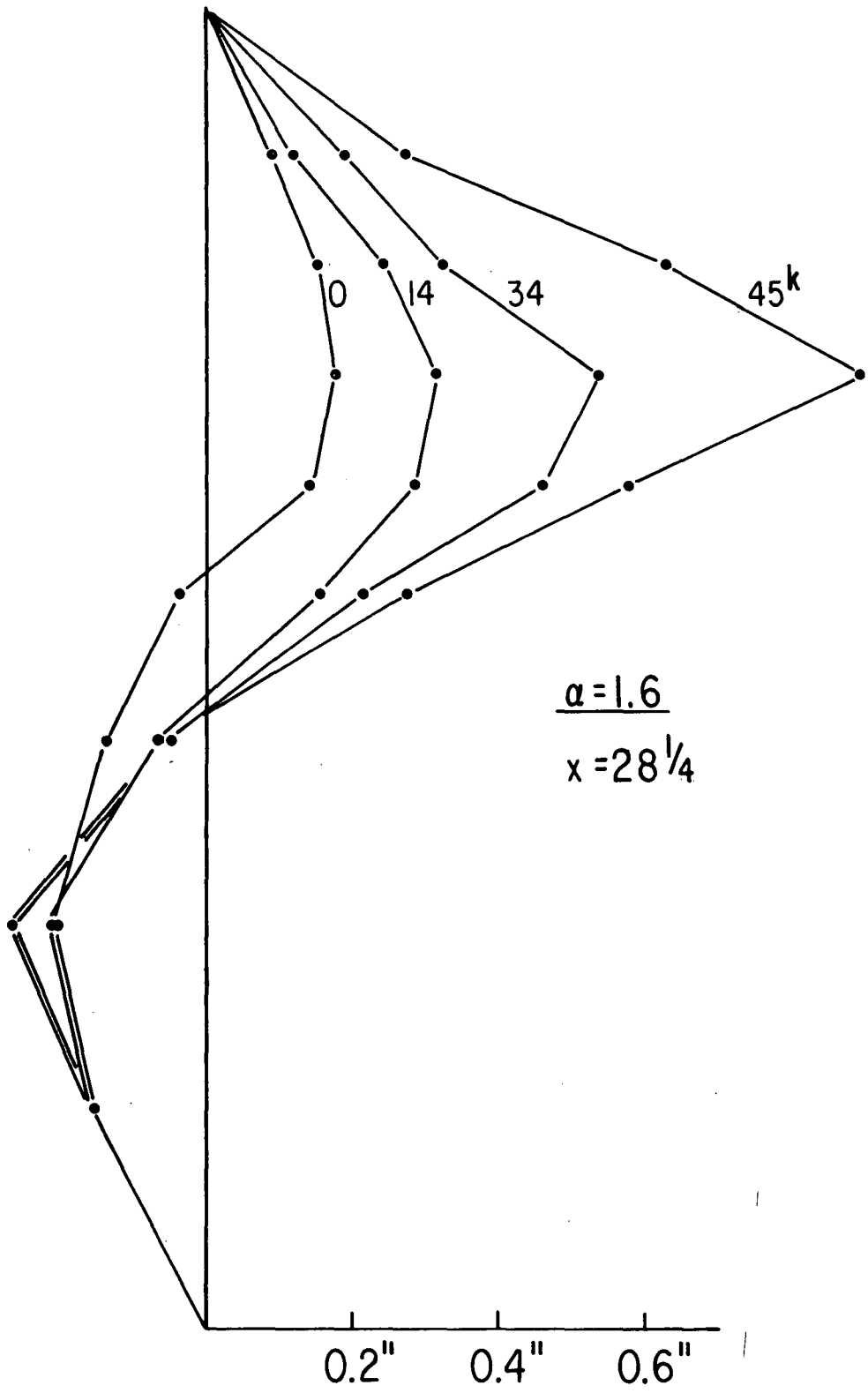

Fig. 31 Progress of Lateral Deflection Near Center of Test Panel, EG-3.1

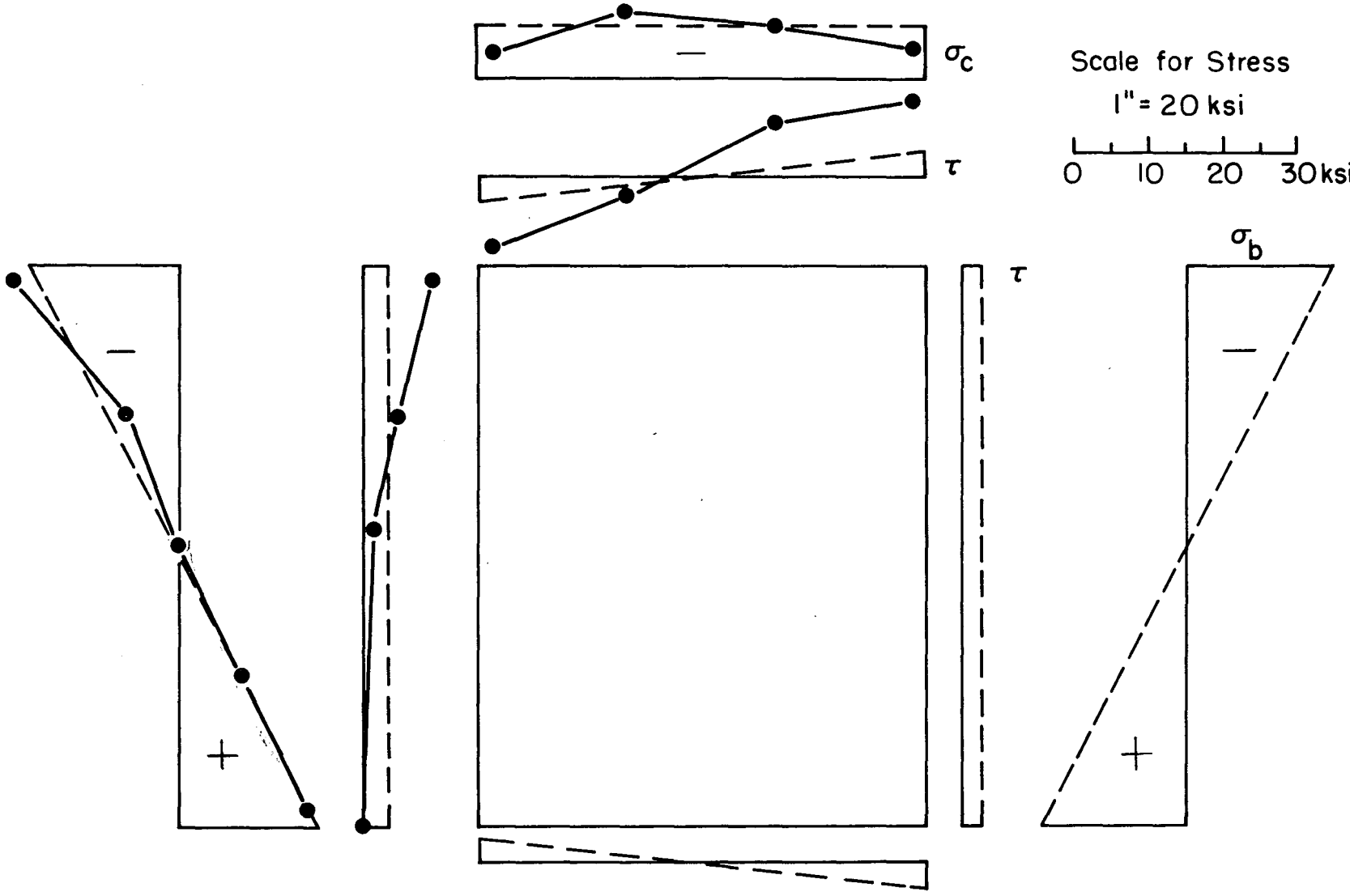

319.1 Fig. 32 Edge Stresses on Test Panel, EG-1.2a

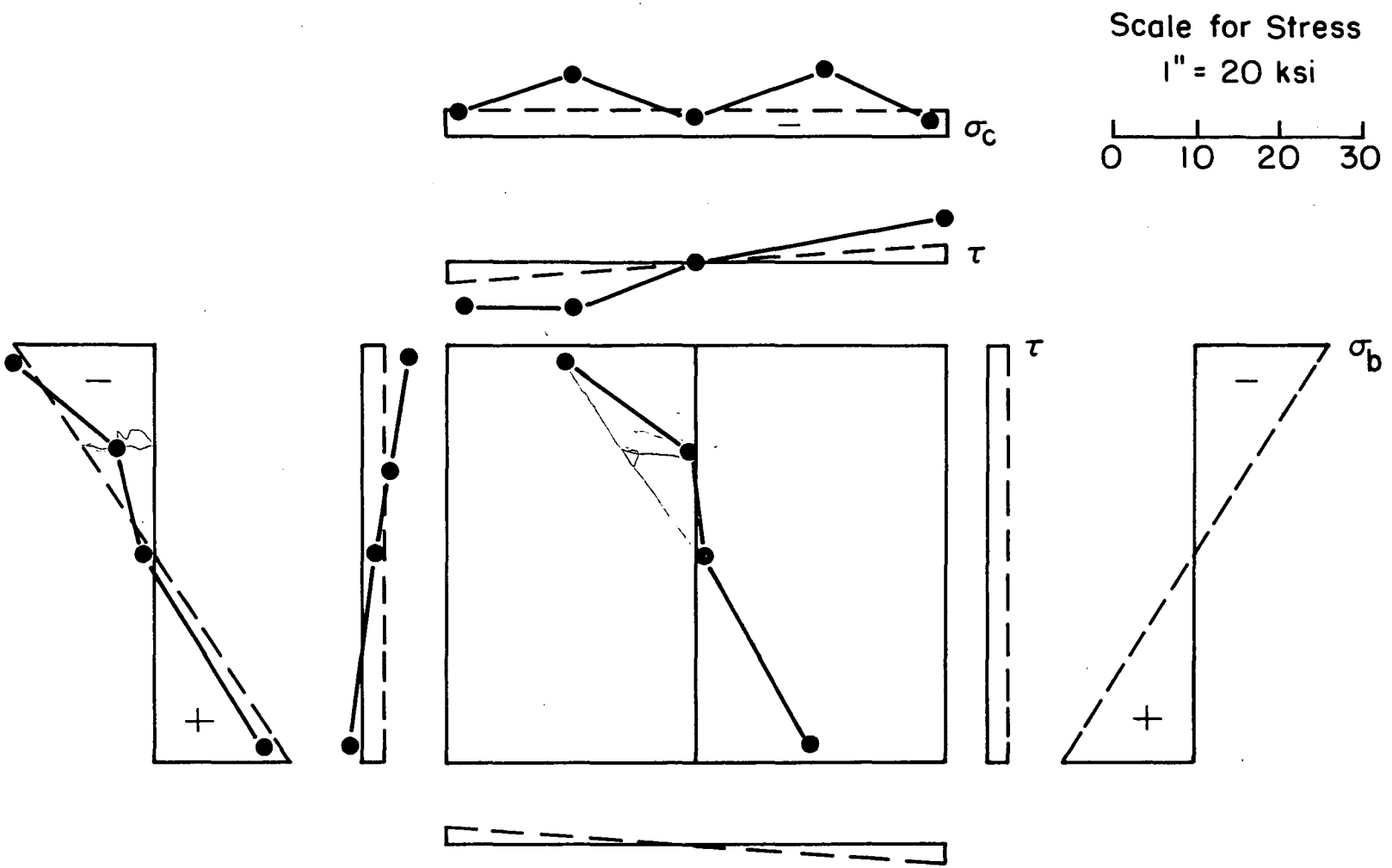

Fig. 33 Edge Stresses on Test Panel, EG-2.1

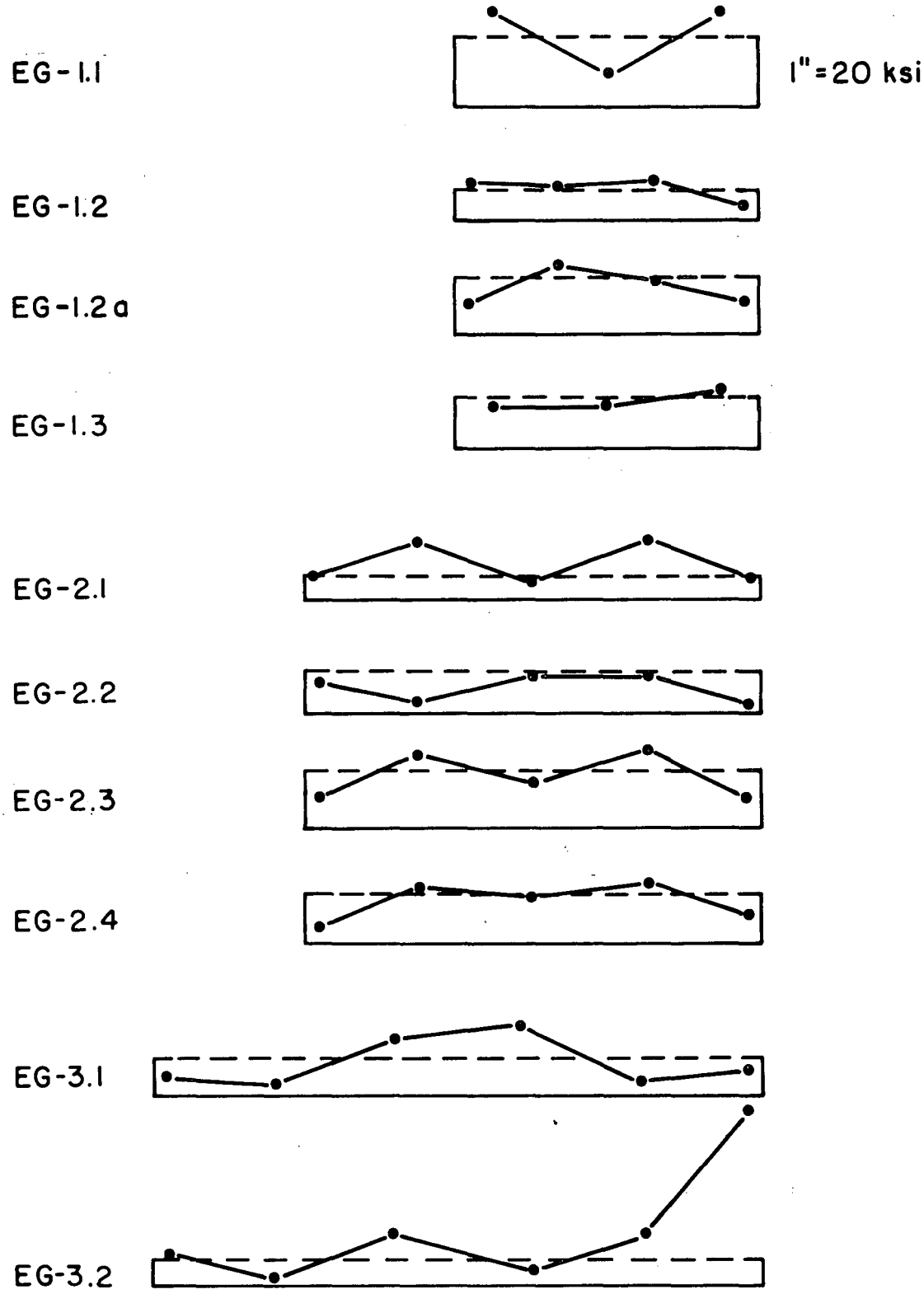

Fig. 34 Vertical Compressive Stress Distribution Over Top Edge of Test Panel

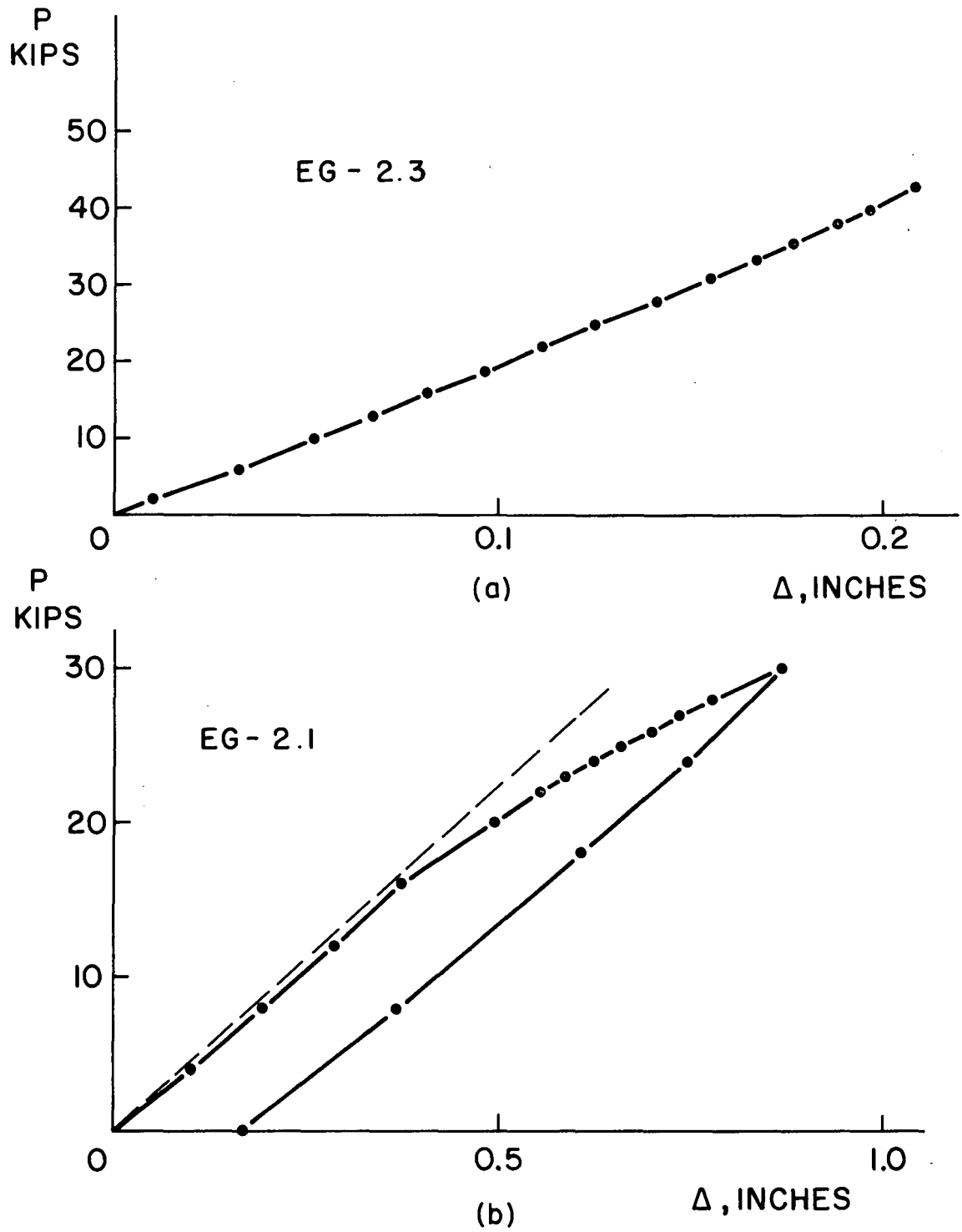

Fig. 35 Load Vs. Vertical Deflection

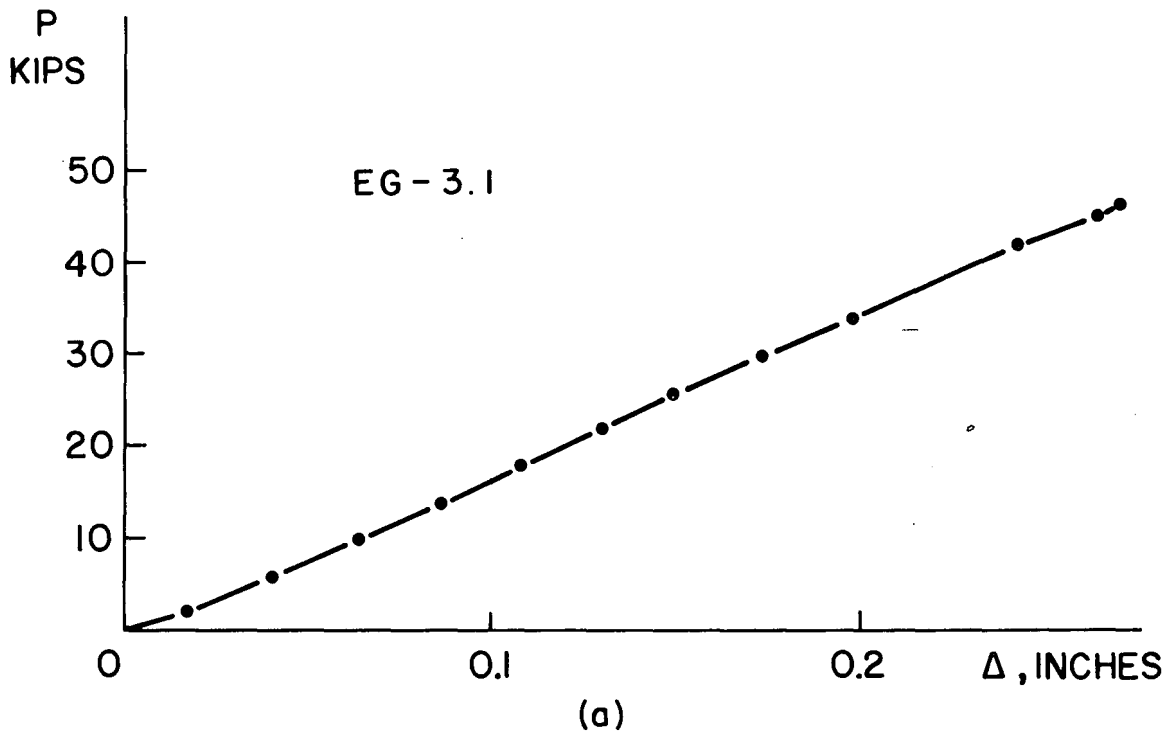

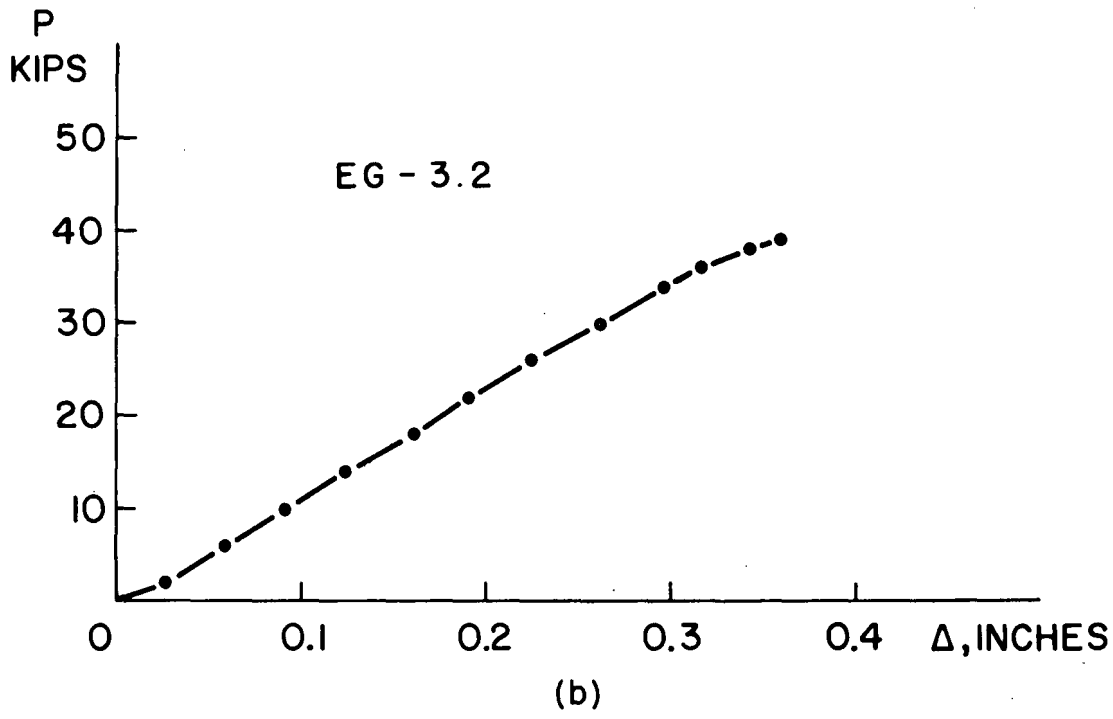

Fig. 36 Load Vs. Vertical Deflection

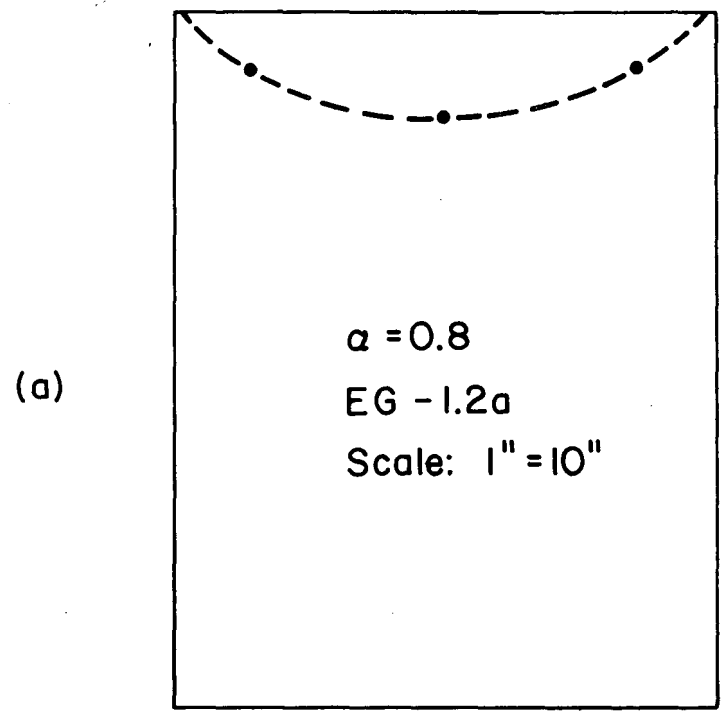

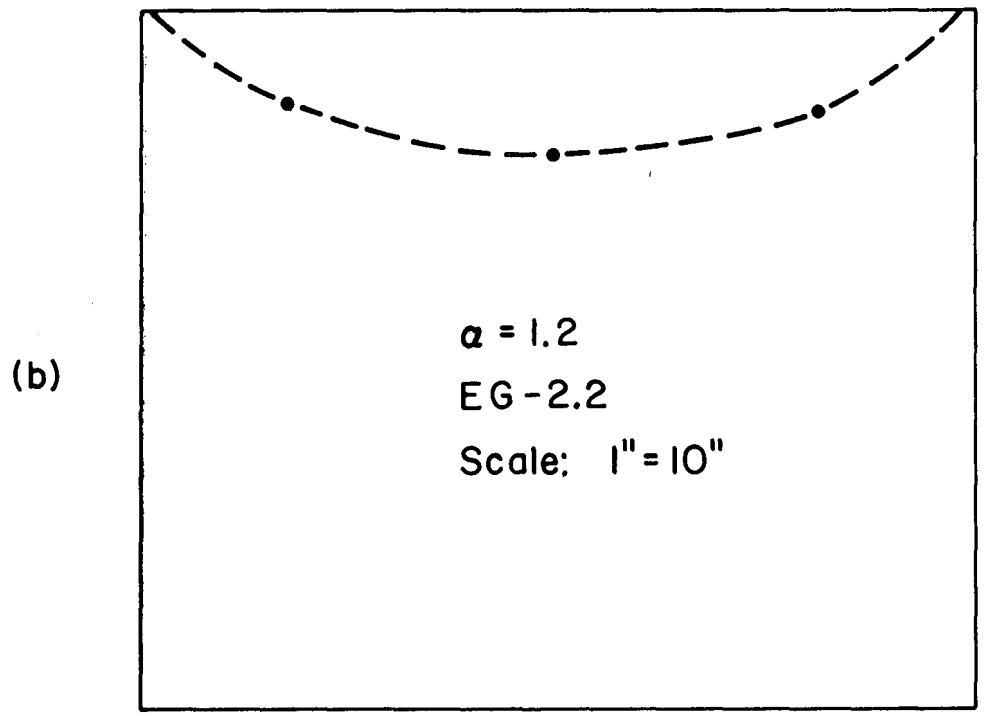

Fig. 37 Yield Bend Location on Test Panels

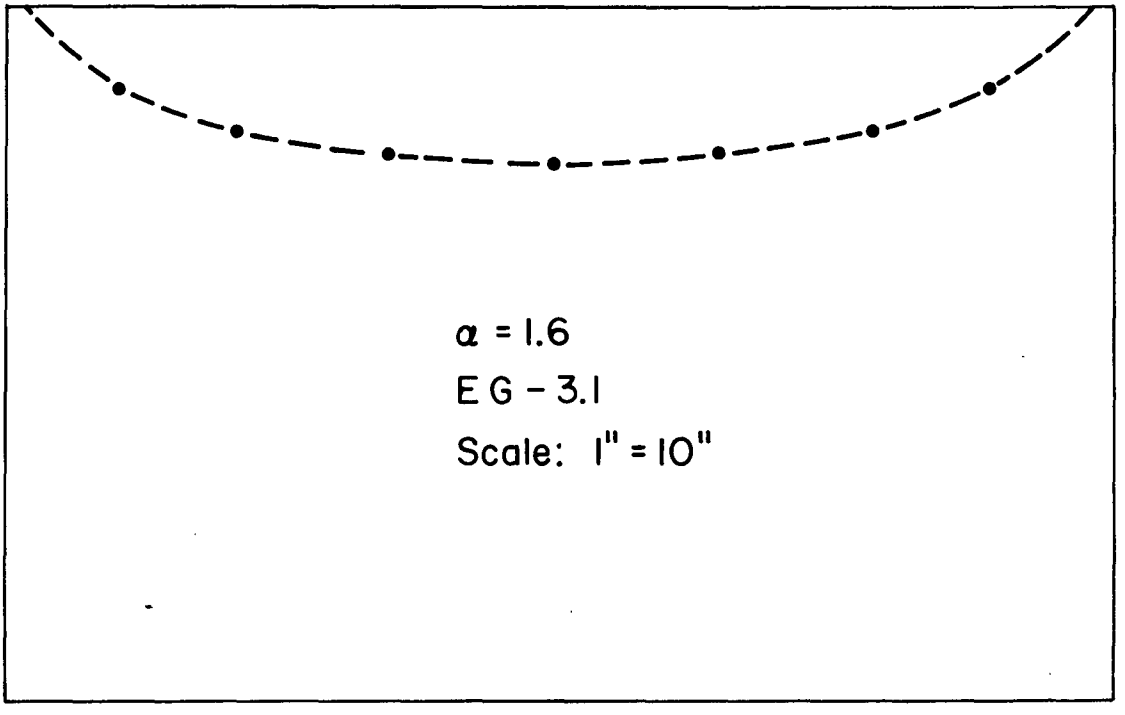

Fig. 38 Yield Bend Location on Test Panel

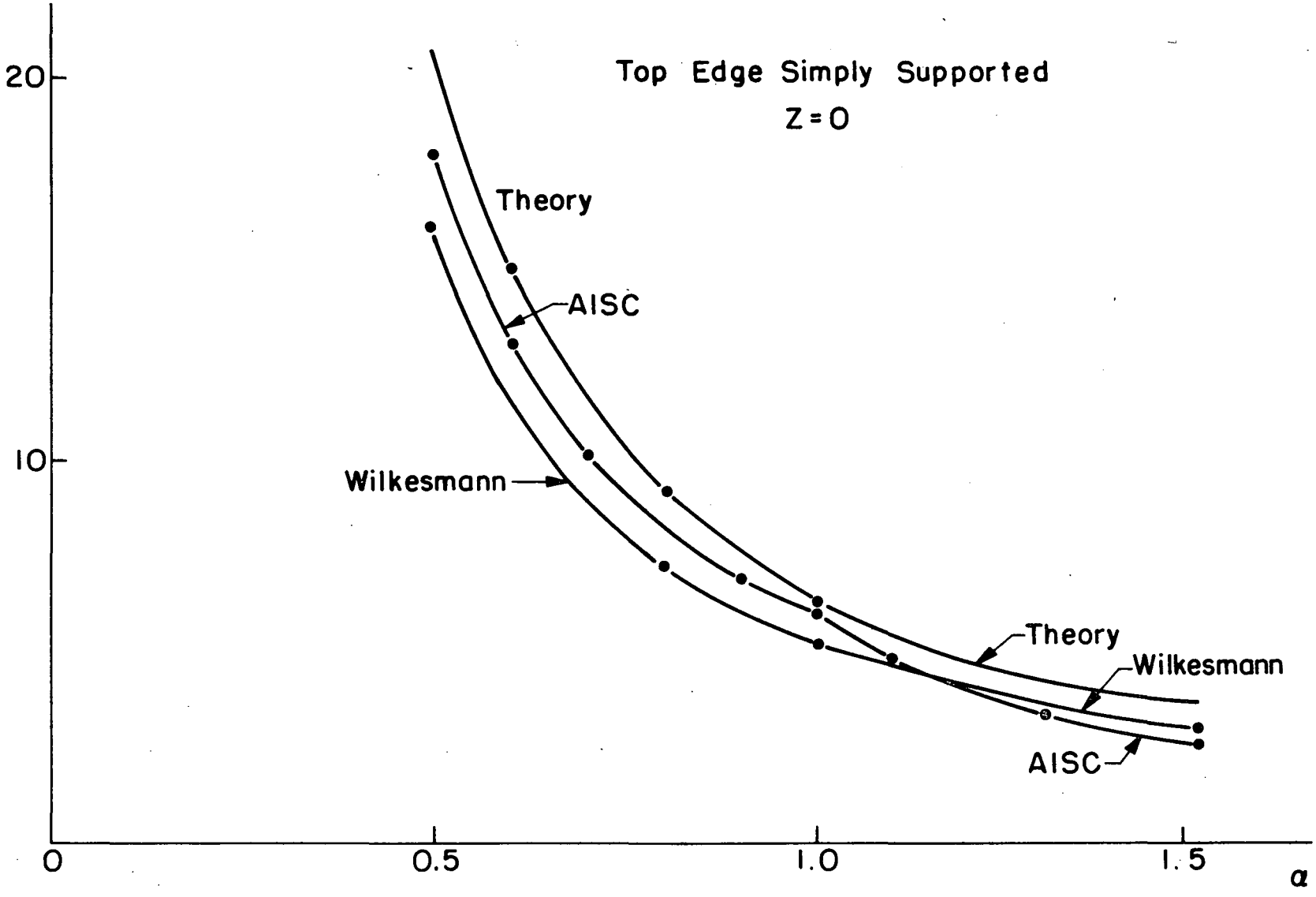

Fig. 39 Comparison of K_{cr} and K_A for Case 1

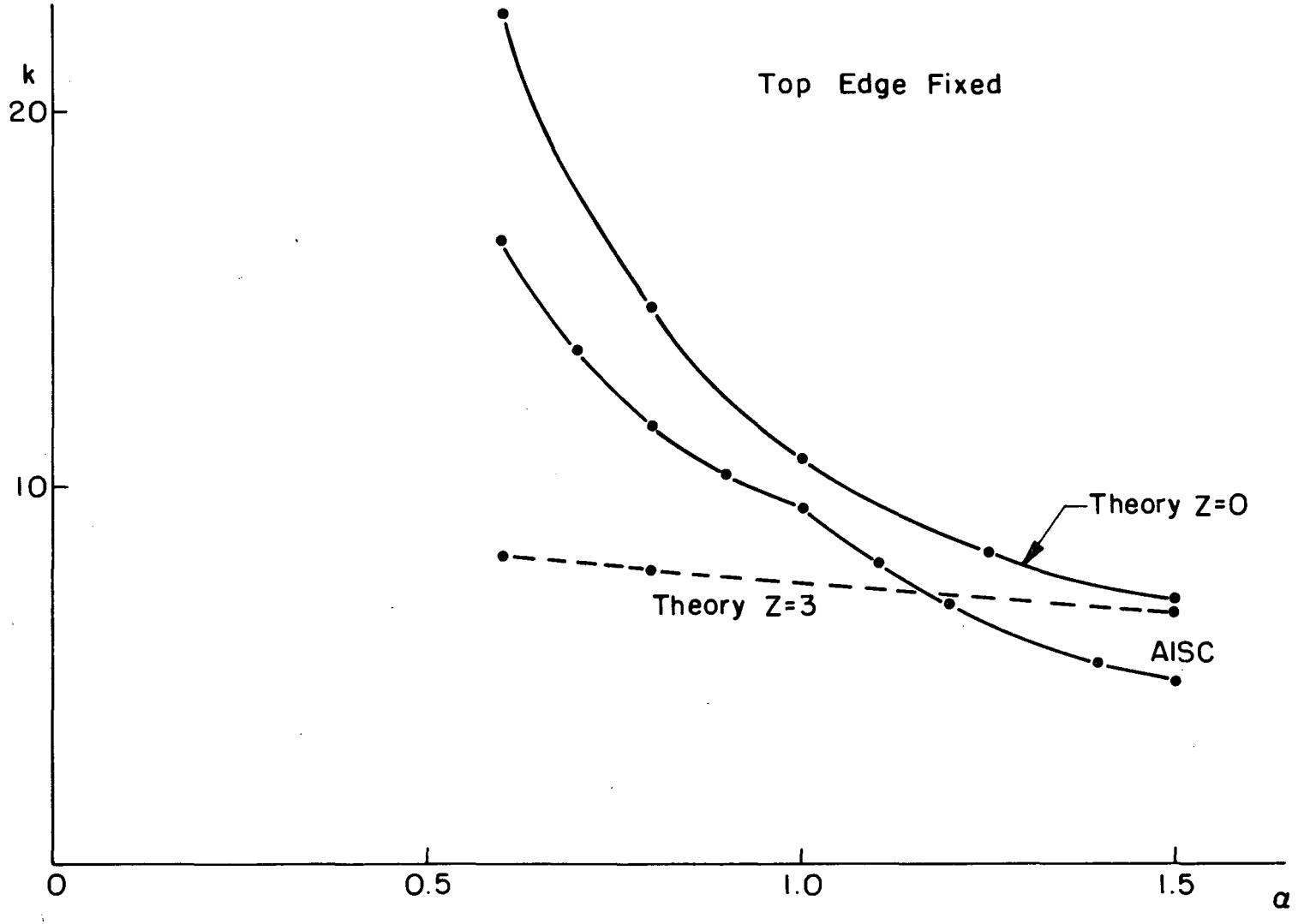

Fig. 40 Comparison of K_{cr} and K_A for Case 2

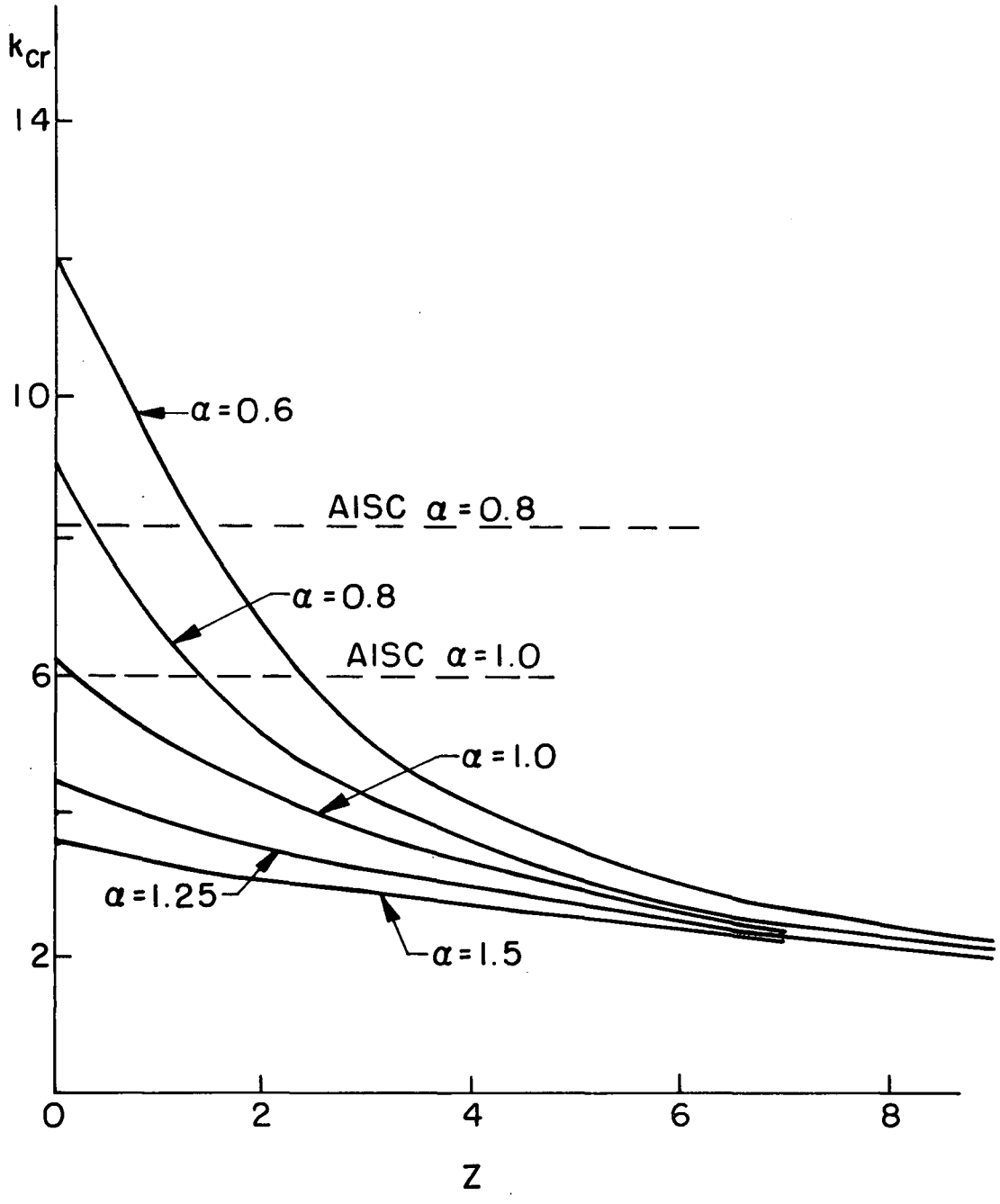

Fig. 41 Variation of K_{cr} with Z and α - Case 1

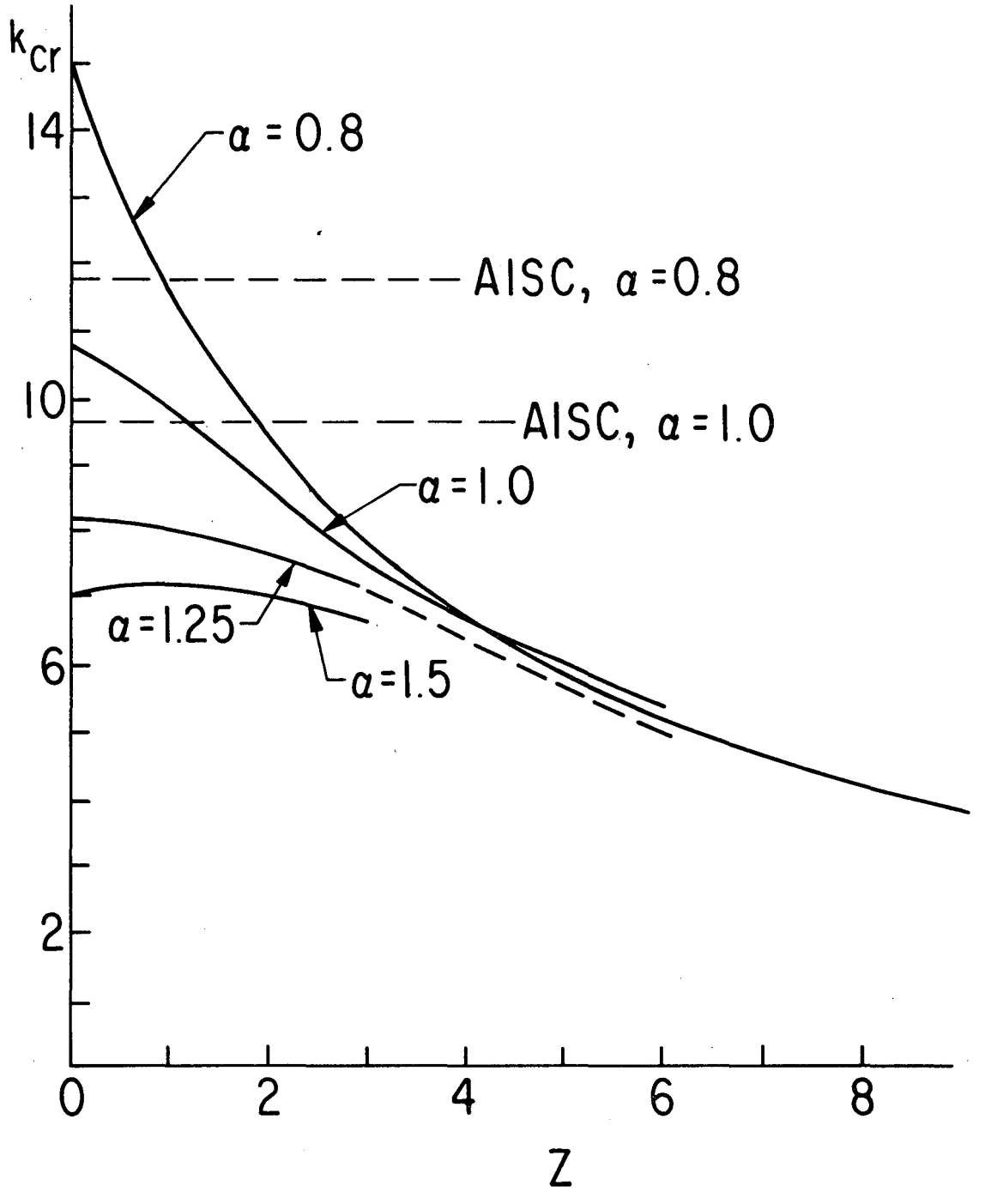

Fig. 42 Variation of K_{cr} with Z and α - Case 2

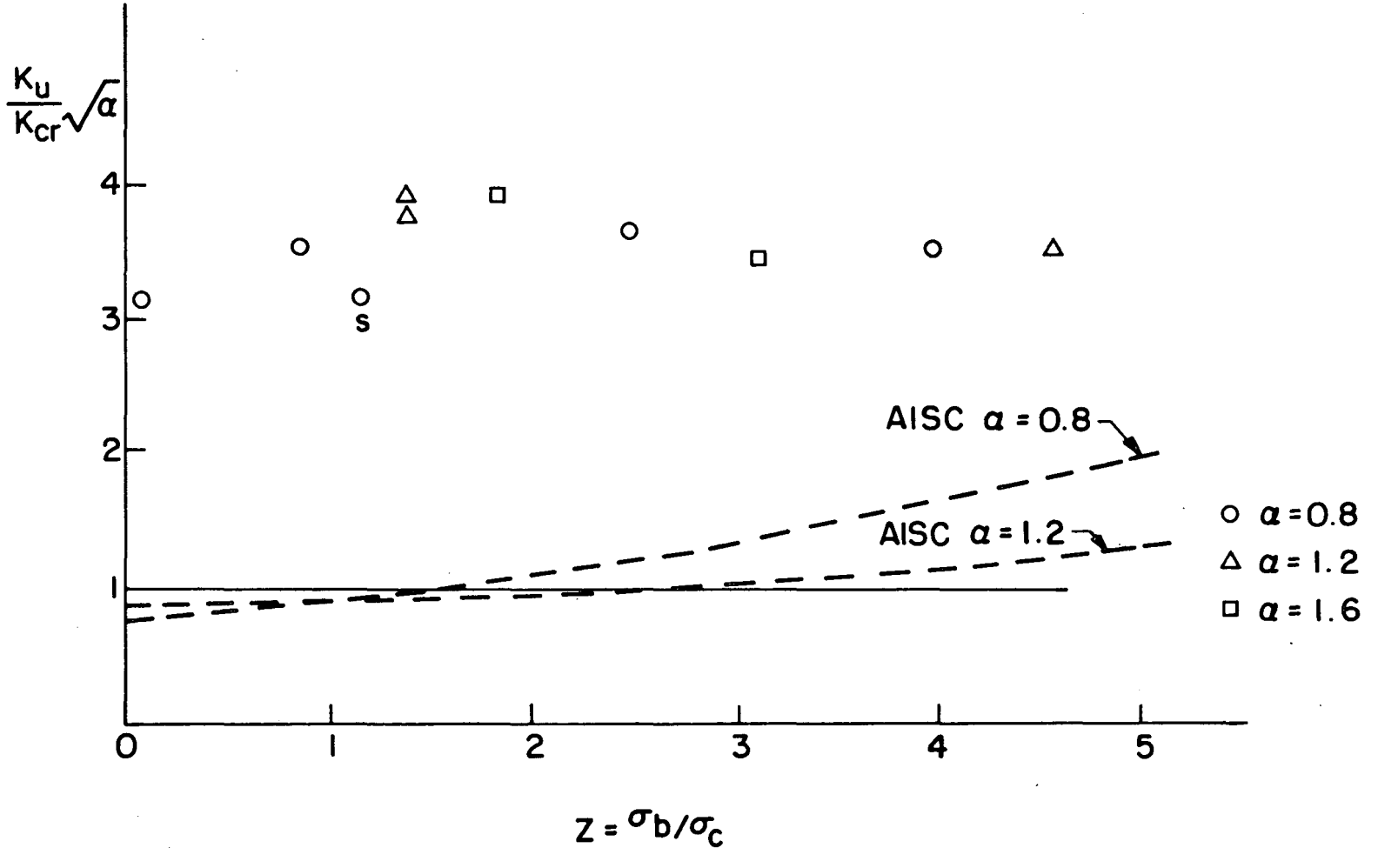

Fig. 43 Variation of $K_u/K_{cr}\sqrt{\alpha}$ with Z

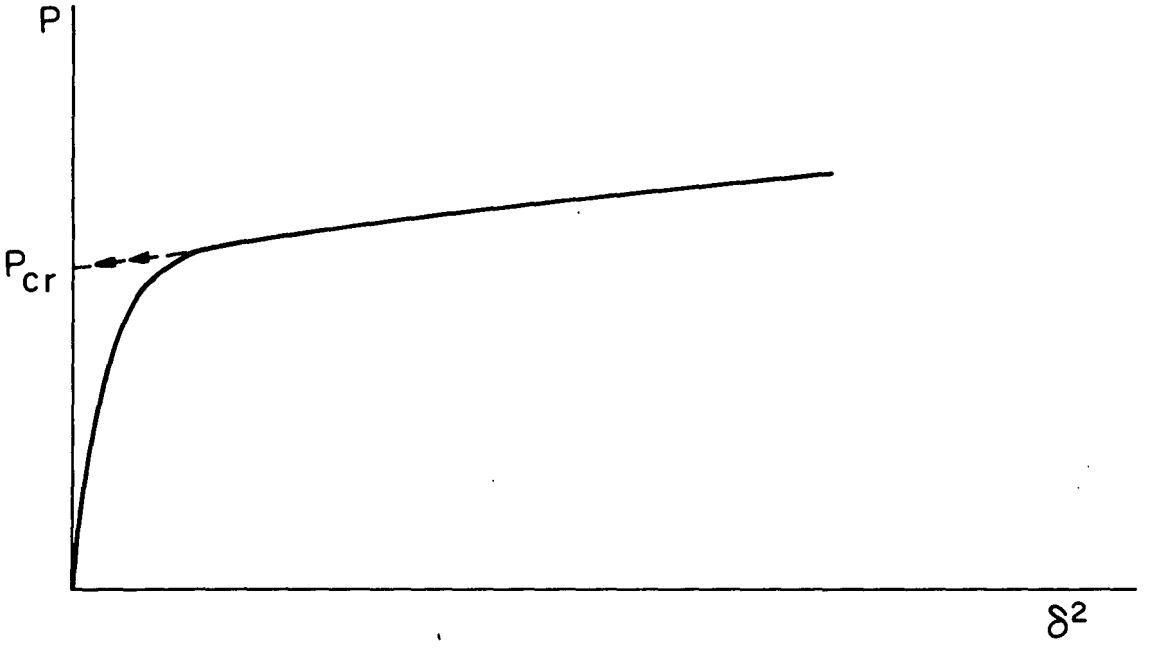

Fig. 44 Ideal P Vs. δ^2 Curve

REFERENCES

1. Wilkesmann, F. W.
   STEGBLECHBEULUNG BEI LANGSTRANDBELASTUNG, Stahlbau (October, 1960)

2. Kloppel, K. and Wagemann, C. H.
   BEULEN EINES BLECHES UNTER EINSEITIGER GLEICHSTRECK-ENLAST, Stahlbau (July, 1964)

3. Warkenthin, W.
   ZUR BEURTEILUNG DER BEULSICHERHEIT QUERBELASTETER STEGBLECHFELDER, Stahlbau (January, 1965)

4. Yoshiki, M.; Ando, N.; Yamamoto, Y.; and Kawai, T.
   STUDIES ON THE BUCKLING STRENGTH OF SHIP STRUCTURES 60th Anniversary Series, The Society of Naval Architects of Japan, Vol. 12, 1966

5. American Institute of Steel Construction
   SPECIFICATION FOR THE DESIGN, FABRICATION, AND ERECTION OF STRUCTURAL STEEL FOR BUILDINGS, AISC, New York, 1963

6. Basler, K.
   NEW PROVISIONS FOR PLATE GIRDER DESIGN, National Engineering Conference Proceedings, AISC, 1961

7. Timoshenko, S. P. and Goodier, J. N.
   THEORY OF ELASTICITY, McGraw-Hill Book Company, New York, 1951

8. Timoshenko, S. P. and Gere, J. M.
   THEORY OF ELASTIC STABILITY, McGraw-Hill Book Company, New York, 1961

9. Yoshiki, M.
   A NEW METHOD OF DETERMINING THE CRITICAL BUCKLING POINTS OF RECTANGULAR PLATES IN COMPRESSION, Journal of Applied Mechanics of Japan, Vol. 3, No. 1, 1947